Coulomb Glasses: A Comparison Between Mean Field and Monte Carlo Results

by

Eivind Bardalen

THESIS

for the degree of

MASTER OF SCIENCE

Condensed Matter Physics

Faculty of Mathematics and Natural Sciences
University of Oslo

June 2011

Det matematisk- naturvitenskapelige fakultet
Universitetet i Oslo

Abstract

In semiconductors at low temperatures, electrons may be localized on impurity centers. Assisted by phonons, conduction is possible by 'hopping' from occupied to unoccupied states.

We study the equilibrium and current properties of such systems numerically, using a two-dimensional lattice model. Results are found using both mean field calculations and Monte Carlo simulations, and a detailed comparison is made of equilibrium and current properties.

It is shown that a modified version of the mean field transition rates yields results which is in better agreement with Monte Carlo results. In the Efros-Shklovskii regime, mean field resistor networks are found to underestimate the conductivity compared to Monte Carlo results. Furthermore, this underestimation can be associated with a longer average jump length compared to Monte Carlo results. This is shown using statistics and mappings of current.

Acknowledgements

The subject of this thesis was suggested to me by Joakim Bergli, who together with Yuri Galperin was my supervisor. I am grateful for the time they have lent me, for the necessary discussions and for showing interest in my work.

Also thanks thanks to the rest of the AMCS group for their friendlyness and office space.

A large amount of literature has been written about the subject. Efros and Shklovskii's book, *Electronic Properties of Doped Semiconductors*, deserves to be especially mentioned, as it has served as the basis for most of what I know about the subject today.

All Monte Carlo simulations in this work were performed with the program written mostly by Martin Kirkengen. In addition, *Matlab* has been a great tool in all my calculations.

Eivind Bardalen
31 May, 2011

'So it goes'
-Kurt Vonnegut

Contents

Notation, Units and Abbreviations

The use of symbols is often a source of confusion, as preferences may vary from author to author. I have done my best to keep notation as consistent and clear as possible, although for some quantities I have used similar symbols ($\nu, N, f, ...$). The most frequently used symbols used in this text are:

- r, $\mathbf{r}$: distance, (distance vector).
- E_f, $\mathbf{E_f}$: Electric field, (electric field vector).
- T: Temperature.
- a: Localization length.
- ϵ_i, ϵ_j, ... : The electron single particle energies at site i, j (or electronic potential).
- ϕ_i, ϕ_j, ... : The on-site energy, defined by equation (3.3).
- $\Phi_{i(j)}$: The single particle energy at site i excluding the interaction with site j.
- $g(\epsilon)$: The density of states.
- Γ_{ij}: The transition rate of jumps from site i to j.
- γ_{ij}: The mean field approximation to Γ_{ij}.
- n_i, n_j, ... : Occupation numbers at sites i, j, ... Possible values are 0 and 1.
- f_i, f_j, ... : The mean field approximations to $\langle n_i \rangle$, $\langle n_j \rangle$, ... with accepted values $0 \leq f_i \leq 1$
- N_{BE}: The Bose-Einstein distribution.
- f_{FD}: The Fermi-Dirac distribution.
- L: Lattice length

The appreviations used in this text are:

- MC: Monte Carlo
- MF: Mean field
- SPE: Single Particle energy.

In the following, except in section 2, we set the ratio of the electron charge to dielectric constant $e/\kappa = 1$ and the Boltzmann constant $k_B = 1$.

In part II, distances r are measured in units of the lattice constant (nearest neighbor distance).

Part I
Theory

1 Introduction

In disordered semiconductors, under certain conditions, the electronic wavefunctions at impurity centers are localized. At lower temperatures, electrons are ejected from the conduction band, and holes from the valence band. They then occupy these localized states.

Depending on the ratio of acceptors to donors, a fraction of the donor states are unoccupied. Then, conduction is due to 'hopping' between localized states, from occupied to unoccupied sites. This hopping is assisted by phonons which cause deformations in the crystal. The availability of phonons follows the Bose-Einstein distribution. Thus, the conductivity of such systems is very temperature-dependent. Furthermore, the transition rate is proportional to the overlap between wavefunctions, which, for hydrogen-type states, decays exponentially.

The original theoretical foundation for such systems is a *mean field* approximation. This approximation reduces all quantities that fluctuate in time to time-independent, averaged ones. Then, in a linear approximation, a pair of sites can be described as a resistor, where the value of the resistor depends on the distance between and the energies of the two sites. The conductivity can then be calculated by that of resistor network.

At temperatures so low that the configuration is close to the ground state, correlations lead to a dip in the density of states at the Fermi level, known as the *Coulomb gap*.

By using resistor networks, the *Efros-Shklovskii* law of conductivity can be derived. At higher temperatures, where there is no Coulomb gap, an equivalent derivation leads to *Mott's law*. In both the Mott and Efros-Shklovskii regimes, a characteristic is the average hopping length, which theoretically increase with lower temperatures. This property has been given the name *'Variable Range Hopping'* (VRH).

Typically, in later years, these systems have been studied numerically using Monte Carlo-type simulations. These simulations, in contrast to mean field theory, take into account the fluctuations of occupation numbers and energies. Thus, correlations in energies and occupation numbers can be exactly described. At low temperatures especially, a disadvantage of Monte Carlo simulations are the long duration times.

The advantage of a mean field approach is its simplicity. Still, concepts and theory from this method is still in use and widely referred to. In e.g. [1], a mean field approach was used to study conductivity properties, and in [2] to study the dynamics.

It is however unclear to what precision mean field theory can be used. In this thesis,

we study the properties of these systems, comparing mean field calculations to Monte Carlo simulations in an attempt to see what and how large the differences are in results using these two methods.

2 Semiconductors

Solid state materials can be divided into three main groups, depending on their electric conductivity: Metals, semiconductors and insulators. These properties can be explained in terms of allowed electronic energy levels in these materials.

2.1 Electronic levels in semiconductors

The allowed energy levels are solutions to the Schrödinger equation:

$$\hat{H}_0\psi_{n,k} = E_{n,k}\psi_{n,k} \tag{2.1}$$

Ignoring electron-electron interactions, $\hat{H}_0$ is

$$\hat{H}_0 = \frac{1}{2m_0}\hat{\mathbf{p}}^2 + V(\mathbf{r}),\ \hat{\mathbf{p}} \equiv -\imath\hbar\vec{\nabla}, \tag{2.2}$$

where $V(\mathbf{r})$ is the periodic potential of the lattice structure and m_0 is the mass of the electron.

Blochs theorem states that the wavefunctions $\psi_{n,k}$ must have the form

$$\psi_{n,k} = e^{i\mathbf{kr}}u_{n,k}(\mathbf{r})\ , \tag{2.3}$$

where $u_{n,\mathbf{k}}(\mathbf{r})$ is a periodic function with the periodicity of the lattice. Analytic solutions to equation (2.1) are possible only for the simplest models. Otherwise, numerical methods are necessary for finding solutions.

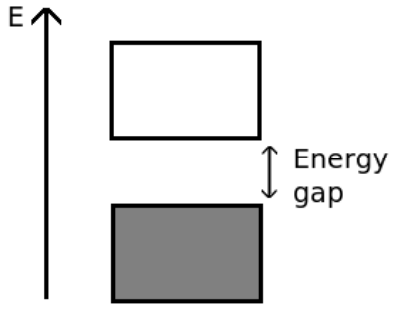

Figure 2.1: Simplified band diagram of a semiconductor. The filled valence band in gray, and the empty conduction band in white.

The n-index in (2.3) refers to the energy band n, while the energy varies continuously with $\mathbf{k}$.

The group velocity of a Bloch electron is

$$\mathbf{v} = \frac{1}{\hbar}\nabla_{\mathbf{k}} E(\mathbf{k}) \tag{2.4}$$

Thus, to create a current, there must be an imbalance in the occupations numbers $f(E_{n,k})$ and $f(E_{n,-k})$. This can only happen if a given band is partially filled.

We refer to the lowest band as the valence band, and the next lowest as the conduction band. If the valence band and conduction band overlap, or if the valence electrons only partly fills the valence band, the material is a metal.

If the valence electrons exactly fill the valence band, and there is a gap between the valence and conduction band, see figure 2.1, depending on the width of energy gap, a crystal is either a semiconductor or insulator. Semiconductors, at room temperature, have a electrical resistivity from $1 \cdot 10^{-3}$ to 10^{9} ohm-cm [3].

2.2 Doping and compensation

By deliberately introducing certain impurities into the host material, the electrical properties of the semiconductor can change significantly. These impurities, or dopants, are divided into two groups: Acceptors and donors.

Acceptors are impurities which, at room temperature, 'capture' one or more electrons from the neighboring atoms, leaving a hole, or the lack of an electron, in the semiconductor. The energy level of the captured electron lies just above the valence band.

Donor electrons, on the other hand, have energies just below the conduction band. They are therefore able to donate electrons to the conduction band, leaving a positive charge at the impurity center.

In semiconductors, at certain temperatures, there is sufficient thermal energy to excite donor electrons into the conduction band, increasing the carrier concentration in the conduction band.

Likewise, valence electrons are easily excited into acceptor states, increasing the carrier concentration in the valence band in the form of holes.

The ratio between the acceptor and donor concentration, we call the *compensation ratio*:

$$K = \frac{N_A}{N_D}\ , \tag{2.5}$$

where N_A, N_D is the acceptor, donor concentration respectively.

2.3 Impurity states

The solutions, $E_{n,k}$, to equation (2.1) typically depends on k in a complicated manner, but for small k (the Brilloun zone center), it is often well described as a free particle with an effective mass m^*:

$$E_n(k) = \frac{\hbar^2 k^2}{2m^*} \tag{2.6}$$

A single impurity acts as a point charge, adding the potential $U = \frac{1}{r}$ to the Hamiltonian:

$$\big(H_0 + U(r)\big)\psi = E\psi \tag{2.7}$$

By expanding ψ in Bloch functions, it can be shown [4] that solutions to ψ are hydrogen type states with energy levels

$$E_t = -\frac{m^*}{2\hbar^2 t^2} \ , \quad t = 1, 2, 3, ... \tag{2.8}$$

E_1 is the *ionization energy* of an isolated impurity, the energy needed to excite the electron into the conduction band, with the wave function

$$\psi = (\pi a^3)^{1/2} e^{-r/a} \ , \tag{2.9}$$

where a is the effective Bohr radius, which henceforth we call the *localization length*,

$$a = \frac{\hbar^2 \kappa}{m^* e^2} \ , \tag{2.10}$$

and κ is the dielectric constant of the material.

2.4 ρ_1 - conductivity

At high temperatures, conductivity is almost entirely dominated by the intrinsic properties of the semiconductors. This is due to the electrons excited across the band gap, E_g. At these temperatures, the density of free electrons/holes is

$$n = p \sim e^{-E_g/2T} \tag{2.11}$$

Lowering the temperature, as the intrinsic carrier concentration decrease, carriers generated from shallow impurities become more important, and may be the dominating source of carriers.

For example, in silicon at room temperature, the addition of 1 boron atom per 10^5 silicon atoms, increases the conductivity by a factor of 10^3 [3].

In the temperature region where carriers are mostly due to ionized impurities, the carrier concentration is given [4] by

$$n \sim e^{-E_1/2T} \ , \tag{2.12}$$

when $KN_D \ll n(T)$, and

$$n \sim e^{-E_1/T} \ , \tag{2.13}$$

when $n(T) \ll KN_D$.

At these temperatures, the conductivity often follows

$$\sigma(T) = \sigma_0 e^{-\epsilon_1/T} \ , \tag{2.14}$$

where ϵ_1 is a number close to the ionization energy.

At even lower temperatures, electrons are recaptured by impurities and conduction is no longer due to free electrons.

3 Semiconductors at Low Temperatures

3.1 Localization

We make the distinction between heavily doped and lightly doped semiconductors based on the conductivity at low temperatures. The conductivity of heavily doped semiconductors are weakly dependent on temperature (metallic), while in lightly doped semiconducturs, it is of the form $\sigma \sim e^{-\epsilon/T}$ (activated) [4].

This difference is due to the character of the impurity states. In heavily doped semiconductors, the states are extended, while in lightly doped semiconductors, they are localized.

The condition for localization is a complicated problem. Anderson, in [5], used the following criterion for localization in lattices: Given a wave function initially as a site function ψ, it is not localized if when the time $t \to \infty$, $\psi(r) \to 0$. If $\psi(r)$ remains finite, it is localized.

In a *lattice* of impurity atoms, localization is a non-trivial problem which depends on the the distribution of site potentials ϵ_i and overlap integrals.

Assuming a wavefunction composed of isolated impurity wavefunctions $\phi(r - r_j)$, solutions to equation (2.7): $\psi(r) = \sum_j a_j \phi_j(r - r_j)$, Anderson's model assumes ϵ_i are evenly distributed in $|\epsilon| < W/2$, in a periodic lattice, such that the Hamiltonian is

$$\hat{H} = \sum_j \epsilon_j a_j^+ a_j + \sum_{j,m\neq 0} I(m) a_j^+ a_{j+m} \ , \tag{3.1}$$

where $I(m)$ is the overlap integral between a site and the m'th nearest neigbor.

For sufficiently large W/I, all electrons are localized, while for smaller W/I, there are only localized states in the tails of the distribution of energies.

3.2 The impurity band structure

A semiconductor can be defined to be *lightly doped* if the overlap integral between neigboring sites is small compared to W. In that case, we can then relate ϵ_i to the

potential due to all other ionized acceptors and donors. Assuming all acceptors have a unit negative charge, the electron potential at a site i is, counted from the isolated-impurity level, E_1, is

$$\epsilon_i = \sum_k^{acceptors} \frac{1}{r_{ik}} + \sum_l^{donors} \frac{n_l - 1}{r_{il}} \tag{3.2}$$

where n_j is the number of electrons at donor j, and $r_{ij} = |\mathbf{r_i} - \mathbf{r_j}|$ is the distance between sites i, j. We will refer to the energies given by (3.2) as the *single particle energies*.

The energy caused by the acceptors, we shall refer to as the *on-site energy*, labelled ϕ. Assuming all acceptors have one negative unit charge,

$$\phi_i = \sum_k^{acceptors} \frac{1}{r_{ik}} \tag{3.3}$$

In lightly doped semiconductors, there are two factors contributing to the dispersion of energy levels. The first is dispersion caused by the wavefunction overlap between impurity states. Due to exponential decay with length, for lightly doped semiconductors, this can be ignored.

The important factor causing dispersion is due to the long-range potential of all ionized donors and acceptors, given by (3.2).

At low ($K \ll 1$) and high ($1 - K \ll 1$) compensation, this leads to a peak in the density of states at the isolated impurity level, like in figure 3.1.

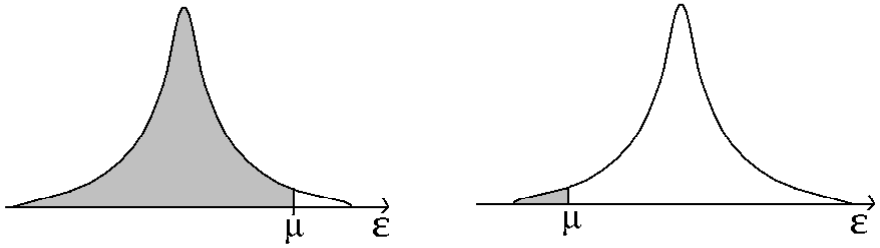

Figure 3.1: The impurity band density of states for a semiconductor with weak compensation (left) and high compensation (right). Shaded area is filled states, white area unfilled states.

Figure 3.1, referring to [4], is qualitatively true, except for states near the Fermi level, μ, where Coulomb interactions may lead to a soft gap in the density of states. For low and high compensations, this gap is small compared to the width of total density of states, while for intermediate compensations, it is large.

In the ground state, the electronic levels given by (3.2) is subject to the following

condition: For a filled site i and an unfilled site j,

$$\epsilon_j - \epsilon_i - \frac{1}{r_{ij}} > 0 \tag{3.4}$$

Or: The energy change in the transition $i \to j$ must be positive. This has important consequences [4]: At the Fermi level, μ, the density of states must be zero. Furthermore, the density of states around the Fermi level must fall at least as $dg(\epsilon)/d\epsilon = \epsilon^2$ (in 3D) or $dg(\epsilon)/d\epsilon = \epsilon$ (in 2D). This leads to a gap in the density of states around μ, known as the *Coulomb gap*.

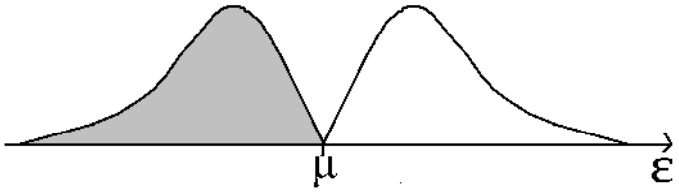

Figure 3.2: The density of states in the ground state for the impurity band with K = 0.5, and $g(\epsilon) \propto |\epsilon|$. Shaded area is filled states, white area unfilled states.

3.3 Miller-Abrahams transition rates

We are interested in the transition rate between localized wavefunctions. In terms of quantum mechanics, transitions from one quantum state $|i\rangle$ to another $|j\rangle$ are possible when there is a perturbation in the Hamiltonian, $\hat{H}'$. In the context of lightly doped semiconductors, $\hat{H}'$ is due to deformations in the material by phonons. The transition rate from a state $|i\rangle$ to a state $|j\rangle$ is then given by Fermi's golden rule:

$$\Gamma_{ij} = \frac{2\pi}{\hbar}\left(\frac{V_0}{8\pi^3}\right)\int d\mathbf{q}\ \delta(\hbar s q - \Delta\epsilon_{ij})|\langle j|\hat{H}'|i\rangle|^2\ , \tag{3.5}$$

where V_0 is the volume, s is the speed of sound and $q = \Delta\epsilon_{ij}/\hbar s$ is the wave vector, where $\Delta\epsilon_{ij}$ is the change in energy in the transition $i \to j$.

The calculation of (3.5) was done in [6], with the result[1]:

$$\Gamma_{ij} = n_i(1-n_j)\frac{E_1^2}{\pi\rho_0 s^5\hbar^4}|\Delta\epsilon_{ij}|I_{ij}^2 N(\Delta\epsilon_{ij})\ , \tag{3.6}$$

[1]It must be noted that other models give other values of the exponent of $|\Delta\epsilon_{ij}|$, e.g. $\Gamma_{ij} \propto |\Delta\epsilon_{ij}|^2 I_{ij} N(\Delta\epsilon_{ij})$

where E_1 is constant describing the deformation potential and ρ_0 is the crystal density. $N(\Delta\epsilon_{ij})$ is the number of phonons with wavevector $q = \Delta\epsilon_{ij}/\hbar s$ and is given by the Bose-Einstein distribution, for a temperature T,

$$N(\Delta\epsilon_{ij}) = N_{BE}(|\Delta\epsilon_{ij}|) = \frac{1}{e^{|\Delta\epsilon_{ij}|/T} - 1} \tag{3.7}$$

for phonon absorption ($\Delta\epsilon_{ij} > 0$), and

$$N(\Delta\epsilon_{ij}) = N_{BE}(|\Delta\epsilon_{ij}|) + 1 \tag{3.8}$$

for phonon emission ($\Delta\epsilon_{ij} < 0$).

I_{ij} is the wavefunction overlap:

$$I_{ij} = -\langle i|\frac{1}{r_i}|j\rangle + \langle i|j\rangle\langle i|\frac{1}{r_j}|j\rangle, \tag{3.9}$$

which, when using hydrogenic wavefunctions and assuming an exactly isotropic mass, averages to

$$I_{ij} = (\frac{2}{3a})(\frac{r_{ij}}{a})\ e^{-r_{ij}/a}\ , \tag{3.10}$$

such that the transition rate from a site i to j is given by

$$\Gamma_{ij} = \frac{E_1^2}{\pi\rho_0 s^5\hbar^4}(\frac{2}{3a^2})^2 r_{ij}^2|\Delta\epsilon_{ij}|e^{-2r_{ij}/a}[N_{BE}(|\Delta\epsilon_{ij}|) + \Theta(-\Delta\epsilon_{ij})]\ , \tag{3.11}$$

where $\Theta(x)$ is the Heaviside step function. The constants are most often, and more convenient, included in a factor ν_0:

$$\Gamma_{ij} = \nu_0\ e^{-2r_{ij}/a}[N_{BE}(|\Delta\epsilon_{ij}|) + \Theta(-\Delta\epsilon_{ij})] \tag{3.12}$$

Relating the change in energy to the the single particle energies $\{\epsilon_i\}$ given by (3.2), for a set of occupation numbers $\{n_i\}$, the change in energy in the transition $i \to j$ is

$$\Delta\epsilon_{ij} = \epsilon_j - \epsilon_i - \frac{1}{r_{ij}}\ , \tag{3.13}$$

where ϵ_j is the energy given by (3.2) *before* the transition, hence the term $1/r_{ij}$ in (3.13).

3.4 Coulomb glasses

Doped semiconductors with strongly disordered, localized states and long-range Coulomb interactions, with transitions due to hopping, often exhibits interesting properties such as $1/f$-noise, see e.g. [7].

Another phenomenom, at such low temperatures that there is a Coulomb gap, is slow relaxations, observed experimentally, see e.g. [8], and in simulations, e.g. [9]. Materials that exhibit this type of glassy behaviour are often called *Coulomb Glasses* or *Electron Glasses*.

3.5 Mean field theory

Analytical theory of Coulomb glasses is difficult, due to the large number of different configurations of occupation numbers $\{n_i\}$. For N_D donors and N_A acceptors, when all acceptors have captured an electron, this number is

$$N = \binom{N_D}{N_A} = \frac{N_D!}{(N_D - N_A)!N_A!} \tag{3.14}$$

Numerical methods, such as Monte Carlo methods, have in the later years been important to the understanding of Coulomb glasses.

The first attempts to estimate the conductivities of such systems, dates back to [6], where the system was treated as a resistance network, where the value of each resistor was given as a function of r and $\Delta\epsilon$. The conductivity was found be

$$\sigma \propto e^{-\epsilon_3/T} , \tag{3.15}$$

by considering linear chains of resistors, where ϵ_3 is some constant. Equation (3.15) is valid only under certain conditions [4].

A *percolation* treatment (percolation is discussed in section 3.6) was used in [10] to show that only states in a small band around the Fermi level contributed to conduction, giving *Mott's* law, in d dimensions:

$$\sigma \propto e^{-(T_0/T)^{1/(d+1)}} \tag{3.16}$$

In [6] and [10], the density of states at the Fermi level was assumed to be constant and non-zero. As mentioned earlier, at low temperatures, there is a Coulomb gap at the Fermi level. Using the same approach as Mott, Efros and Shklovskii, showed that this leads to, independent of dimension,

$$\sigma \propto e^{-(T_0/T)^{1/2}} , \tag{3.17}$$

known as the *Efros-Shklovskii* (ES) law.

3.5.1 The mean field equations

The derivation of equations (3.16) and (3.17) is made assuming a specific form of the density of states, $g(\epsilon)$: $g(\epsilon) = g_0$ and $g(\epsilon) = \alpha|\epsilon|^{(dimension-1)}$ respectively. The latter correspond to the ground state, while the former correspond to a temperature where the Coulomb gap has vanished.

Thermal fluctuations can be incorporated in the energies using a mean field approach. In mean field theory, as an approximation, the time-dependence in equations (3.11) and (3.2) can be replaced by time-averaged quantities. These quantities are given by a set of equations which we from hereon will call the *mean field equations*.

These equations are [4]:

- Single particle energies and occupation numbers:

$$\epsilon_i = \phi_i + \sum_{j \neq i} \frac{f_j}{r_{ij}}, \tag{3.18}$$

where the set $\{f_i\}$ are the mean occupation numbers determined by the Fermi-Dirac distribution:

$$f_i = f_{FD}(\epsilon_i) = \frac{1}{e^{\epsilon_i/T} + 1} \tag{3.19}$$

For a system with N sites, the set $\{\epsilon_1, \epsilon_2, ...\epsilon_N\}$ given by equation (3.18) forms a self-consistent set of N number of equations.

- Transition rates:

By replacing time-fluctuating single particle energies (3.2) with the approximation (3.18), the change in energy in the transition $i \to j$ is

$$\Delta\epsilon_{ij} = \epsilon_j - \epsilon_i, \tag{3.20}$$

and we obtain expressions for the average transition rates between sites, $\langle n_i(1 - n_j)\Gamma_{ij}\rangle$. Labelling the mean field rates γ, these are, for a pair of sites i, j:

$$\gamma_{ij} = \nu_0 \; f_i(1 - f_j)e^{-2r_{ij}/a}[N_{BE}(|\Delta\epsilon_{ij}|) + \Theta(-\Delta\epsilon_{ij})] \tag{3.21}$$

In equilibrium, these are balanced: $\gamma_{ij} = \gamma_{ji}$.

This approximation must have some limitations. As Efros and Shklovskii writes in [4], "(...), for intermediate compensation or for variable-range hopping conductivity the above approximation is not justifiable. In our view this lead to an unknown numerical factor in the exponent characterizing the temperature dependence of the electrical conductivity".

Here, we focus on exactly variable range hopping. Still, we will use the equations above in our later calculations, as was also done in [1]. A more sophisticated set of equations is exists, which also follows [4], is described in section 3.5.3.

3.5.2 Formulation of a resistance network

The equations in section 3.5 applies to a closed system. In an open system with an applied external electric field $\mathbf{E_f}$, the balance between transition rates is upset, creating a current.

In a linear approximation, the system can be reformulated as a resistance network [4]. Following this derivation, ignoring the energy dependence of ν_0:

The electric field redistributes the electrons over donors. In a weak field, these corrections can be considered small: $f_i = f_i^0 + \delta f_i$. In addition to the electric field, the change in occupation numbers of all donors in turn causes small changes in site energies:

$$\delta\epsilon_i = \mathbf{E_f} \cdot \mathbf{r} + \sum_{j \neq i} \frac{\delta f_j}{r_{ij}} \tag{3.22}$$

The change in occupation numbers can be expressed as a change in the local chemical potential:

$$f_i(E) = f_i^0 + \delta f_i = \frac{1}{1 + e^{\frac{\epsilon_i - \delta\mu_i}{T}}} \tag{3.23}$$

In an open circuit, $\delta\mu = -\delta\epsilon$, and there is no net flow. In a closed circuit, $\delta\mu \neq -\delta\epsilon$, with a resulting imbalance $\gamma_{ij} \neq \gamma_{ji}$, where

$$\begin{aligned} \gamma_{ij} &= \gamma_{ij}^0 + \delta\gamma_{ij} \\ \gamma_{ji} &= \gamma_{ji}^0 + \delta\gamma_{ji} \end{aligned} \tag{3.24}$$

$\gamma_{ij}^0 = \gamma_{ji}^0$ are the transition rates in equilibrium. The net current from site i to site j is then

$$J_{ij} = -(\delta\gamma_{ij} - \delta\gamma_{ji}) \tag{3.25}$$

$\delta\gamma_{ij}$ can be obtained by expanding γ_{ij} to first order:

$$\delta\gamma_{ij} = \frac{\partial}{\partial f_i}\gamma_{ij}^0\delta f_i\Big|_{f_i^0} + \frac{\partial}{\partial f_j}\gamma_{ij}^0\delta f_j\Big|_{f_j^0} + \frac{\partial}{\partial\Delta\epsilon_{ij}}\gamma_{ij}^0\delta(\Delta\epsilon_{ij})\Big|_{\Delta\epsilon_{ij}^0} \tag{3.26}$$

For a negative energy transition $\Delta\epsilon_{ij} < 0$, this is

$$\delta\gamma_{ij} = \frac{1}{f_i^0}\gamma_{ij}^0\delta f_i - \frac{1}{1 - f_j^0}\gamma_{ij}^0\delta f_j + \frac{1}{1 + N_{BE}}\frac{dN_{BE}}{d\Delta\epsilon}\gamma_{ij}^0\delta\Delta\epsilon_{ij}, \tag{3.27}$$

where

$$\frac{dN_{BE}}{dE} = -N_{BE}^2\frac{e^{\Delta\epsilon/T}}{T}$$

Furthermore, using the relation

$$N_{BE}(\Delta\epsilon)e^{\Delta\epsilon/T} = 1 + N_{BE}(\Delta\epsilon)$$

we eventually get

$$\delta\gamma_{ij} = \frac{1}{f_i^0}\gamma_{ij}^0\ \delta f_i - \frac{1}{1 - f_j^0}\gamma_{ij}^0\ \delta f_j - \frac{N_{BE}}{T}\gamma_{ij}^0\ \delta\Delta\epsilon_{ij}\ , \tag{3.28}$$

while for the opposite transition

$$\delta\gamma_{ji} = -\frac{1}{1-f_i^0}\gamma_{ij}^0\ \delta f_i + \frac{1}{f_j^0}\gamma_{ij}^0\ \delta f_j + \frac{1}{N_{BE}}\frac{dN_{BE}}{dE}\gamma_{ij}^0\ \delta\Delta\epsilon_{ji}\ , \tag{3.29}$$

which becomes

$$\delta\gamma_{ji} = -\frac{1}{1-f_i^0}\gamma_{ij}^0\ \delta f_i + \frac{1}{f_j^0}\gamma_{ij}^0\ \delta f_j - \frac{N_{BE}+1}{T}\gamma_{ij}^0\ \delta\Delta\epsilon_{ij} \tag{3.30}$$

We then get an expression for the current from site i to j:

$$\begin{aligned} J_{ij} &= -(\delta\gamma_{ij} - \delta\gamma_{ji}) \\ &= \gamma_{ij}^0\left[\big(\delta f_i^0(\frac{1}{f_i^0} - \frac{1}{1-f_i^0}) + \delta f_j^0(-\frac{1}{f_j^0} + \frac{1}{1-f_j^0}) + \frac{\delta\Delta\epsilon_{ij}}{T}\right] \end{aligned} \tag{3.31}$$

The linear corrections to f_i can be expressed in terms of the adjusted chemical potential μ_i:

$$\delta f_i \approx \frac{\partial f_i}{\partial\mu_i}\delta\mu_i = -\frac{e^{\epsilon_i^0/T}}{T}(f_i^0)^2\delta\mu_i = \frac{(1-f_i^0)f_i^0}{T}\delta\mu_i\ , \tag{3.32}$$

such that the end result is

$$J_{ij} = -\frac{\gamma_{ij}^0}{T}\big(\delta\mu_j - \delta\mu_i + \delta\epsilon_j - \delta\epsilon_i\big) \tag{3.33}$$

Current conservation requires:

$$\sum_{j\neq i} J_{ij} = 0 \tag{3.34}$$

Thus, the quantities $\delta\mu_i + \delta\epsilon_i$ can be associated with the value of the local electrochemical potential U_i at each site, $(\delta\mu_i + \delta\epsilon_i = U_i)$:

$$J_{ij} = -\frac{\gamma_{ij}^0}{T}(U_i - U_j) \tag{3.35}$$

Thus, the linear response to a weak electric field enables the system to be formulated as a resistance network where each resistance

$$R_{ij} = \frac{T}{\gamma_{ij}^0} \tag{3.36}$$

is determined from equilibrium solutions of the system.

3.5.3 Modification of transition rates and the resistor network

The mean field equations, (3.18), and (3.19), give sets of average occupation numbers and single-particle energies. At low temperatures, it is clear that these solutions must tend to some pseudo-stable state. By pseudo-stable, we mean a configuration which is stable against one-particle jumps. At these temperatures, where ϵ_i, ϵ_j, $\Delta\epsilon_{ij} \gg T$, the mean field transition rates are, to a good approximation,

$$\gamma_{ij} \approx \nu_0 \; e^{-2r_{ij}/a - \epsilon_{ij}/T} \; , \tag{3.37}$$

where

$$\epsilon_{ij} = \begin{cases} \max\{|\epsilon_i|, |\epsilon_j|\} & , \epsilon_i \cdot \epsilon_j > 0 \\ |\epsilon_j - \epsilon_i| & , \epsilon_i \cdot \epsilon_j < 0 \end{cases} \tag{3.38}$$

At these temperatures, a Coulomb gap has been formed at the Fermi level. Thus, jumps across the Fermi level must account for a large part of transitions. In fact, when the system is in its ground state, these jumps are the *only* allowed jumps.

However, Equation (3.37) indicates that there is a preference for jumps on the same side of the Fermi level. This is due to the definition of the mean field transition rates, equation (3.21).

For energies $|\epsilon_i| >> T$, f_i must be close to 0/1 for states above/below the Fermi level. Then, for a transition from a negative energy site i to a positive energy site j, the change in energy $\Delta\epsilon_{ij}$ includes the contribution from the occupied state i. This is an unphysical self-interaction.

To see this more clearly, consider the change in energy in a transition between a pair of sites:

$$\Delta\epsilon_{ij} = \epsilon_j - \epsilon_i = (\phi_j + \frac{f_i}{r_{ij}} + \sum_{k \neq i,j} \frac{f_k}{r_{jk}}) - (\phi_i + \frac{f_j}{r_{ij}} + \sum_{k \neq i,j} \frac{f_k}{r_{ik}}) \tag{3.39}$$

The two terms, f_i/r_{ij} and f_j/r_{ij}, in equation (3.39), is a contribution from the sites themselves.

In the exact case, a transition is the transfer of one electron from site i to site j. In that case, (exchanging occupation numbers, $f_i \rightarrow n_i$) the expression in the first parentheses must be the energy at site j *after* the transition, and the expression in the second parenthesis is the energy at site i *before* the transition, in which case $n_i = n_j = 0$. Thus, equation (3.39) is only a good approximation if $|f_i - f_j| \ll 1$.

For a pair of sites are both on the same side of the Fermi level: $(\epsilon_i \cdot \epsilon_j > 0)$, this results in the appropriate change in energy. When $\epsilon_i, \epsilon_j > 0$, $f_i, f_j \approx 1$ and when

$\epsilon_i, \epsilon_j < 0$, $f_i, f_j \ll 1$, such that

$$\Delta\epsilon_{ij} \approx \phi_j + \sum_{k\neq i,j} \frac{f_k}{r_{jk}} - \phi_i + \sum_{k\neq i,j} \frac{f_k}{r_{ik}}$$

In the opposite case, for a pair of sites both on opposite side of the Fermi level ($\epsilon_i \cdot \epsilon_j < 0$), the result is

$$\Delta\epsilon_{ij} \approx \phi_j + \sum_{k\neq i,j} \frac{f_k}{r_{jk}} - \phi_i - \sum_{k\neq i,j} \frac{f_k}{r_{ik}} + \frac{f_j - f_i}{r_{ij}}$$

$f_j - f_i \approx -1$ for downwards transitions, and $f_j - f_i \approx 1$ for upwards transitions. Thus, there is an additional term, an unphysical contribution to the energy change. If $\Delta\epsilon^0$ is the exact change: $\Delta\epsilon_{ij} \approx \Delta\epsilon^0 \pm \frac{1}{r_{ij}}$.

At low temperatures after the formation of the Coulomb gap, the magnitude of this term is limited by the condition of a pseudo-stable state: Any transition from a filled state i to an unfilled state j must have a positive energy change: $\epsilon_j - \epsilon_i > 1/r_{ij}$, which sets a limitation on the minimal distance between these states:

$$r_{ij} > \frac{1}{\epsilon_j - \epsilon_i},$$

which is of the order of the energy change $\Delta\epsilon_{ij}$.

The issue of self-interaction can be resolved by using a modified version of the transition rates. In [4], the following derivation were for a system in the ground state configuration. We will use the same derivation, but for *any* configuration. Following [4], we use the following reasoning:

Assuming the system is in some configuration, with the sites i and j initially empty. We can then assume the occupation probability on sites i, j follows a function $F(n_i, n_j)$. This probability depends on the energy change $E(n_i, n_j)$ in the system with the addition of (n_i, n_j) electrons.

Defining

$$\Phi_{i(j)} = \epsilon_i + \sum_{k\neq i,j} \frac{f_k}{r_{k,i}} \tag{3.40}$$

as the single particle energy at site i excluding the contribution from neighbor j, the energy change is,

$$E(n_i, n_j) = \begin{cases} 0, & (n_i, n_j) = (0, 0) \\ \Phi_{i(j)}, & (n_i, n_j) = (1, 0) \\ \Phi_{j(i)}, & (n_i, n_j) = (0, 1) \\ \Phi_{j(i)} + \Phi_{i(j)} + 1/r_{ij}, & (n_i, n_j) = (1, 1) \end{cases} \tag{3.41}$$

and $F(n_i, n_j)$ must be

$$F(n_i, n_j) = \frac{1}{Z_{ij}} \exp\left[-\frac{1}{T}(\Phi_{i(j)} n_i + \Phi_{j(i)} n_j + \frac{1}{r_{ij}} n_i n_j)\right] \tag{3.42}$$

where $1/Z_{ij}$ is the normalization constant, the inverse of the partition function of the two-site system:

$$Z_{ij} = 1 + e^{-\frac{\Phi_{i(j)}}{T}} + e^{-\frac{\Phi_{j(i)}}{T}} + e^{-\frac{\Phi_{i(j)}+\Phi_{j(i)}+1/r}{T}} \tag{3.43}$$

The transition rate from i to j then must follow

$$\gamma_{ij} = F(1,0)\ \nu_0\ e^{-2r_{ij}/a}\big[N_{BE}(|\Delta\Phi_{i(j)}|) + \Theta(-\Delta\Phi_{i(j)}))\big] \tag{3.44}$$

These rates are balanced in equilibrium: $\gamma^0_{ij} = \gamma^0_{ji}$. An external electric field upsets this balance, creating a net current in the system. By following a derivation like that in 3.5.3, it can be shown that the result is a resistance network, where the resistances R_{ij} now are given by

$$R_{ij} = \frac{T}{\gamma^0_{ij}} \tag{3.45}$$

where γ^0_{ij} is given by equation (3.44). At low temperatures $\Phi_{i(j)}, \Phi_{j(i)}$ and $\Delta\Phi_{i(j)} \gg T$, this can be approximated to, omitting the superscript,

$$\gamma_{ij} \approx \nu_0\ e^{-2r_{ij}/a - \epsilon_{ij}/T}, \tag{3.46}$$

which is the same as eq. (3.37), except for an additional $1/r$ term for jumps across the Fermi level:

$$\epsilon_{ij} = \begin{cases} \max\{|\epsilon_i|, |\epsilon_j|\}\ , \ \epsilon_i \cdot \epsilon_j > 0 \\ |\epsilon_j - \epsilon_i| - \frac{1}{r_{ij}}\ , \ \epsilon_i \cdot \epsilon_j < 0 \end{cases} . \tag{3.47}$$

3.6 Percolation

In the previous sections, we saw how the mean field approximation allowed the formulation of a resistance network. When doing calculations of the conductivity, this approximation offers a great reduction in complexity compared to the equations formulated in section 3.3.

Solving the resistance network, however, still is not trivial, at least not analytically. In later sections, we find numerical solutions of the resistance networks. Here, we will briefly introduce percolation theory, which provides one way to estimate the conductivity.

Percolation theory has its origin as a mathematical problem in the 1950s, and can often be related to physical systems, e.g. ferromagnetic materials and flow in porous

media. Such systems can often be described by sites connected by bonds. By allowing some of these bonds or a sites to be switched on, depending on some probability x, there will be a formation of connected sites, clusters. At the critical value x_c, there should a formation of an infinite cluster.

In a finite system, we are often interested in the treshold for percolation between opposite sides.

3.6.1 Estimation of conductivity by percolation

Percolation theory produces a framework for conductivity calculations, if we the relate bonds to the resistors: $R_{ij} = R_0 e^{\xi_{ij}}$. We assume that the range of values of ξ is large (compared to 1).

If we remove all resistors with a ξ-value less than ξ', there must be some value $\xi' = \xi_c$, in which an infinite cluster of sites first is formed. The value for ξ_c, we call the *percolation threshold*.

The networks consisting of resistors with $\xi' < \xi_c$ form a number of isolated clusters, while the crucial connections between clusters are made of resistors with $\xi' \sim \xi_c$. The *critical subnetwork* is the network consisting of these resistors. For this network, a usual limitation on ξ' is $\xi' < \xi_c + 1$.

It is now reasonable to assume that the total conductivity is largely determined by the the resistors with $\xi \sim \xi_c$. The argument for this is that while the network with $\xi' < \xi_c$ make up the bulk of the network, their resistance is low compared to the connections between clusters.

Since these connections are made by resistors with $\xi \sim \xi_c$, they should also largely determine the conductivity of the total system, while resistors with $\xi >> \xi_c$ cannot be of significance, because of the exponential dependence on ξ; They are shorted by the critical subnetwork.

This reasoning leads to the following expression for the conductivity

$$\sigma = 1/\rho = \sigma_0 e^{-\xi_c} \tag{3.48}$$

Thus, if ξ depends on temperature, the temperature dependence , $\sigma(T)$, can be found by finding an expression for the percolation threshold ξ_c.

3.6.2 The Efros-Shklovskii law

At low temperatures ($\epsilon_i, \Delta\epsilon_{ij} \gg T$), equation (3.21) can be approximated

$$\gamma_{ij} = \nu_0 \; e^{-\frac{2r_{ij}}{a} - \frac{\epsilon_{ij}}{T}} = \nu_0 \; e^{\xi_{ij}} \;, \tag{3.49}$$

with ϵ_{ij} given by equation (3.38), such that the pair-wise resistances, in this approximation, are given by equation (3.36),

$$R_{ij} \propto e^{\frac{2r_{ij}}{a} + \frac{\epsilon_{ij}}{T}} \tag{3.50}$$

Assuming that the conductivity of the total network is determined by the ξ-value of the critical resistor,

$$\sigma \approx \sigma_0 e^{-\xi_c} \ , \tag{3.51}$$

the problem consists of estimating the value of the critical resistance $R_c \propto e^{\xi_c}$.

From the percolation threshold ξ_c, there are limiting values for ϵ and r:

$$\epsilon_{\max} = \xi_c \ T \tag{3.52}$$

$$r_{\max} = \frac{a}{2}\xi_c \tag{3.53}$$

We now assume that the density of states vanish at the Fermi level, and near the Fermi level is described by: $g(\epsilon) = \alpha|\epsilon|^{d-1}$, where α is some constant and d is the spatial dimension, the concentration of sites with $\xi < \xi_c$ is

$$n_c = n(\xi_c) = \int_0^{r_{max}} d^d r \int_{-\epsilon_{max}}^{\epsilon_{max}} d\epsilon \ g(\epsilon) = \frac{\alpha}{d} r_{max}^d \ 2\epsilon_{max}^d \tag{3.54}$$

Using equations (3.52) and (3.53) in equation (3.54), we get the expression for the critical value of ξ, when $d = 2$:

$$\xi_c = (\frac{4n_c}{a^2 T^2})^{1/4} = (\frac{T_0}{T})^{1/2} \tag{3.55}$$

where $T_0 = \beta/a$, with $\beta = 2\sqrt{n_c}$. In general, β must be determined numerically.

The jump length corresponding to the critical resistance is

$$r_c = \frac{a}{2}(\frac{T_0}{T})^{1/2} \tag{3.56}$$

Part II
Modelling and Numerics

In part I, the basic theory of Coulomb glasses was presented.

The purpose of this parts III and IV is to make a comparison between results obtained from mean field theory and results from Monte Carlo simulations.

In this part, we describe the model, the Monte Carlo program used, and the numerics of the mean field calculations.

4 The 2D Lattice Model

To model the system of electrons in a Coulomb glass in 2 dimensions, the donor sites are placed on a square lattice, with sides of length $L = 100$, with distance 1 between nearest neighbors, such that the system contains $N = L^2 = 10^4$ donor sites.

To each site i, we attribute a constant potential energy ϕ_i, from a uniform, random distribution in the interval $[-1, 1]$. This is the on-site disorder energies caused by charged acceptors, given by equation (3.3). The same disorder configuration is used in all calculations in both mean field and Monte Carlo simulations, unless as specified.

To account for the negative charge at the acceptors, we add a constant background charge $\nu = 0.5$. This charge corresponds to half filling, or $N/2 = 5000$ electrons in the Monte Carlo simulations.

In order to remove edge effects, we use periodic boundary conditions in both directions, such that the electrons both interact with sites on opposite sides and are free to jump across sides. An exception to this are the resistor networks used in mean field current calculations. Here, a cut is made between vertical sides, and with the electric field in the x-direction.

For faster calculations, we set the maximum allowed jump length to 10, and the Coulomb interactions are cut after a distance of $L/2$ to avoid self-interaction.

The expressions for the single particle energies are then

$$\epsilon_i = \phi_i + \sum_{j \neq i} \frac{n_j - 0.5}{r_{ij}} \tag{4.1}$$

in Monte Carlo simulations, and

$$\epsilon_i = \phi_i + \sum_{j \neq i} \frac{f_j - 0.5}{r_{ij}} \tag{4.2}$$

in mean field calculations.

For the transition rates γ_{ij} and Γ_{ij}, we set the preexponential factor $\nu_0 = |\Delta\epsilon_{ij}|/t_0$, such that

$$\Gamma_{ij} = \frac{|\Delta\epsilon_{ij}|}{t_0} e^{-2r_{ij}/a}[N_{BE}(|\Delta\epsilon_{ij}|) + \Theta(-\Delta\epsilon_{ij})] \tag{4.3}$$

for the Monte Carlo rates in the simulations.

The unmodified mean field transition rates (of section 3.5) in this model are

$$\gamma_{ij} = \frac{|\epsilon_i - \epsilon_j|}{t_0} f_i(1-f_j) e^{-2r_{ij}/a}[N_{BE}(|\Delta\epsilon_{ij}|) + \Theta(-\Delta\epsilon_{ij})] \ , \tag{4.4}$$

while the modified transition rates are

$$\gamma_{ij} = \frac{|\Phi_{i(j)} - \Phi_{j(i)}|}{t_0} F(1,0) e^{-2r_{ij}/a}(N(|\Phi_{i(j)} - \Phi_{j(i)}|) + \Theta(-\Phi_{j(i)} + \Phi_{i(j)})) \ , \tag{4.5}$$

where $F(1,0)$, is given by equation (3.42).

In the following, we set $t_0 = 1$, which defines the timescale. In all calculations, a localization length $a = 1$ is used.

5 On Monte Carlo Simulations

Assuming a system that follows the equations in section 3.3, where the time-evolution is described in terms of transition rates between configurations, the time-averaged probabilities $\{P_I\}$ of finding the state in a given configuration I, is found by solving the master equation:

$$\frac{dP_I}{dt} = \sum_{J \neq I} (P_J \Gamma_{JI} - P_I \Gamma_{IJ}) \tag{5.1}$$

where Γ_{IJ} is the transition rate between configurations I and J. Solving (5.1) gives the exact values of P_I.

Since the number of possible configurations I in a system with n electrons and N sites is $\frac{N!}{(N-n)!n!}$, finding an analytical solution of the master equation, quickly becomes an impossible task.

An alternative to solving the master equation is Monte Carlo simulations. This is a method for evolving the system from an initial configuration by choosing transitions depending on likelyhood.

In this thesis, we use Monte Carlo simulations as approximations to the exact solutions.

5.1 Description of program and algorithm

The program used to obtain Monte Carlo results has previously been written by Andreas Glatz and Martin Kirkengen in C++. A more detailed description of the program can be found in [11]. Here follows a short description of the algorithm used.

The foundation of the algorithm is based on an idea in [12], which splits the transition rate Γ_{ij} in two factors:

$$\Gamma_{ij} \propto \Gamma_{ij}^T \Gamma_{ij}^A \tag{5.2}$$

The transition rate Γ_{ij} depends on a tunneling probability:

$$\Gamma_{ij}^T = e^{-2r_{ij}/a} \tag{5.3}$$

and a probability which depends on the activation by phonons:

$$\Gamma_{ij}^A = |\Delta\epsilon| \big(\frac{1}{e^{|\Delta\epsilon_{ij}|/T} - 1} + \Theta(-\Delta\epsilon_{ij}) \big) \tag{5.4}$$

$\Delta\epsilon_{ij}$ is again the change in energy. In an applied external electric field, this is

$$\Delta\epsilon_{ij} = \epsilon_j - \epsilon_i - \frac{1}{r_{ij}} - \mathbf{E_f} \Delta \mathbf{r}_{ij} \tag{5.5}$$

Since the sites are placed on a lattice with no disorder in position, Γ^T needs only to be calculated once. This is a computational advantage, as calculations are faster.

The initial configuration is defined in the user input, and is either random or set to a given configuration. The time-evolution from this initial configuration, are determined from *Monte Carlo cycles*.

In a Monte Carlo cycle, a transition is either accepted or rejected, according to the steps below:

- 1: For a random site i, if it contains an electron, using a probability distribution, weighted by Γ_{ij}^T, an empty neighbor j is chosen.
- 2: The activation rate Γ_{ij}^A for the chosen pair i,j is calculated, and accepted with a probability depending on Γ_{ij}^A and a number P_m, described below. If rejected, the program restarts the cycle.

The number of Monte Carlo cycles N_{MCs} before a jump is accepted defines the time spent in the configuration. This time is given by

$$t = t_{MC}\ N_{MCs} \tag{5.6}$$

where

$$t_{MC} = \frac{1}{L^2 K P_m \sum \Gamma_{ij}^T} \tag{5.7}$$

where L is the lattice length, K is the compensation, and the summation is over neigbors closer than the maximum jump length.

The role of P_m is as a cut-off parameter in the acceptance probability of a jump, see figure 5.1. Any suggested jump with $\Gamma_{ij}^A > P_m T$ is accepted, while it is accepted with a probability $P = P_m T\ \Gamma^A$ if $\Gamma_{ij}^A < P_m T$. This is necessary, as in our model, Γ^A is monotonically increasing to infinity at negative ϵ, which in itself is unphysical.

P_m may be interpretated as a cutoff in in the possible frequencies of phonons, determined by the crystal lattice constant l and s, the speed of sound in the crystal:

$$|\Delta\epsilon| \leq \frac{hs}{2l} \tag{5.8}$$

5.1.1 Choice of parameters

A proper discussion of the parameters in the Monte Carlo program was given in [11]. The main results are given below.

- For Ohmic conductance, the electric field strength, E_f, should be less than 1/10 of the temperature.
- In the non-Ohmic regime, the choice of P_m influenced the conductivity calculations. In the Ohmic regime, there was no significant difference between $P_m = 3, 20, 50$.

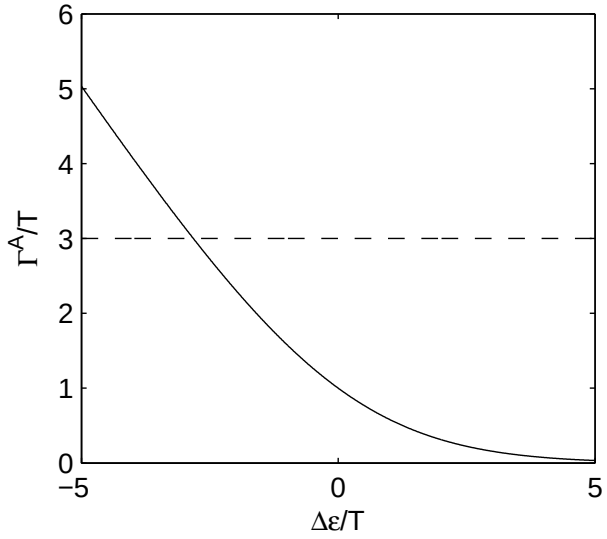

Figure 5.1: Full line: Activation probability Γ^A. Dashed line: The cut-off probability $P_m T$, here set to 3.

Using the results above, in this thesis, we choose $P_m = 3$, and for the simulations with an applied electric field, we use $E_f = T/10$.

6 Mean Field Solutions

6.1 Numerical solutions of the mean field equations

The mean field SPE energies, given by equations (3.18) and (3.19) require numerical methods to be solved. Here, we find solutions by an iterative procedure:

- We start with some set of initial values: $(\epsilon_1, \epsilon_2, ..., \epsilon_N)_1$. either random or specified.
- We declare a new set of energies, identical to the initial: $(\epsilon_1, \epsilon_2, ..., \epsilon_N)_2$=$(\epsilon_1, \epsilon_2, ..., \epsilon_N)_1$
- In a random order of sites $i = \{1, 2, .., 10^4\}$, new values $(\epsilon_i)_2$ are calculated as

$$(\epsilon_i)_2 = \phi_i + \sum_{\substack{j \neq i, where \\ r_{ij} < L/2}} \frac{(f_j)_2 - 0.5}{r_{ij}} \tag{6.1}$$

  The new value of $(\epsilon_i)_2$ replaces the old value in the set $(\epsilon_1, \epsilon_2, ..., \epsilon_N)_2$ before the next value is calculated.

- After all energies have been calculated, we check for convergence by calculating the change $\sum_i \delta\epsilon_i = \sum_i |(\epsilon_i)_2 - (\epsilon_i)_1|$. If $\sum_i \delta\epsilon_i$ is smaller than some threshold value (using $\sum_i \delta\epsilon_i < 1 \cdot 10^{-6}$ for a 100x100 lattice), the new set of energies is accepted as a solution. If not, the previous step is repeated, with $(\epsilon_1, \epsilon_2, ..., \epsilon_N)_1$ replaced by $(\epsilon_1, \epsilon_2, ..., \epsilon_N)_2$.

6.2 Calculation of current in the mean field approximation

The transition rates between sites for the system without electric field determine the resistances $\{R_{ij}\}$ between sites. Then, all sites form a resistance network with with widely varying resistances. In our two-dimensional model, the sites on the left boundary are set to a constant potential V, and all sites on the right boundary are set to a zero potential.

In the following, potentials are labelled U and conductances $\tilde{\Gamma}$ $(= 1/R)$.

Kirchoffs laws determine the potential at each site. At each site, flow in must equal flow out:

$$\sum_{j \neq i} J_{ij} = \sum_{j \neq i} (U_j - U_i)\, \tilde{\Gamma}_{ij} = 0 \tag{6.2}$$

or

$$\sum_{j \neq i} \tilde{\Gamma}_{ij} U_j - (\sum_{j \neq i} \tilde{\Gamma}_{ij}) U_i = 0 \tag{6.3}$$

Since the potential at the boundaries is known:

$$\sum_{j \neq i, j \notin i_B} \tilde{\Gamma}_{ij} U_j - (\sum_{j \neq i} \tilde{\Gamma}_{ij}) U_i = V \sum_{j \in i_{LB}} \tilde{\Gamma}_{ij} + 0 \sum_{j \in i_{RB}} \tilde{\Gamma}_{ij} \tag{6.4}$$

Here, i_B, i_{LB}, i_{RB} mean site belonging to left or right boundary, left boundary and right boundary, respectively.

Equation 6.4 can be rewritten as a matrix equation $\mathbf{Gu} = \mathbf{b}$ with $(N^2 - 2N)(N^2 - 2N)$ elements and where the diagonal elements $G_{i,i}$ are given by

$$G_{ii} = -\sum_{j \neq i} \tilde{\Gamma}_{ij} \ , \tag{6.5}$$

and the off-diagonal elements are given by

$$G_{ij} = \tilde{\Gamma}_{ij} \tag{6.6}$$

The right-hand side elements of B are

$$b_i = V \sum_{j \in i_{LB}} \tilde{\Gamma}_{ij} \tag{6.7}$$

Matrix inversion of $\mathbf{G}$ yields the potentials $\mathbf{u} = \mathbf{G}^{-1}\mathbf{b}$. (This is done in Matlab using `U=G\B`).

The total current is found from

$$J_{tot} = \sum_{i \in i_{LB}} \sum_{j \notin i_{LB}} (V - U_j)\tilde{\Gamma}_{ij} \tag{6.8}$$

In a 100x100 lattice, the total number of conductances is about 1 million, of which only a small part (10000-100000) are appreciably large. The rest can in practice be omitted without any sizeable change in the results.

Part III
Equilibrium Properties

In this section, equilibrium properties, that is, the properties of the system when in thermal equilibrium, and in the absence of an external electric field, are investigated.

7 Equilibrium in Monte Carlo Simulations

It is necessary to include a discussion to define what is meant by equilibrium in the context of Coulomb glasses.

In the canonical ensemble [2], two systems are said to be in equilibrium if there is, on average, no net flow of energy between the two.

In systems where the individual energies of particles are uncorrelated, such as in an ideal gas, in thermal equilibrium, the occupation probability of the particles (in the case of fermions) follows a Fermi-Dirac distribution:

$$f_{FD}(\epsilon_i) = \frac{1}{e^{\frac{\epsilon_i - \mu}{T}} + 1} \tag{7.1}$$

Since the mean field equations are defined in terms of (7.1), where the particle energies (ϵ_i) are

$$\epsilon_i = \phi_i + \sum_{j \neq i} \frac{f_j}{r_{i,j}} \ ,$$

it should be clear that any solution of the mean field equations can be treated as an equilibrium solution.

Still, this does not deal with the fact that there many solutions to the mean field equations, and increasingly so at low temperatures. Then one could argue that not all mean field solutions should be treated equally. For the moment we will leave this question aside.

More problematic is the question of thermal equilibrium in Monte Carlo simulations. Coulomb glasses are characterized by the correlated behaviour of the electrons. Here, electrons interact with the surroundings by emitting and absorbing phonons. Long range $1/r$ interaction combined with exponentially decaying (with distance) transition probabilities sometimes makes a necessary relaxation difficult.

[2] In the canonical ensemble, two systems are allowed to exchange energy, but not particles.

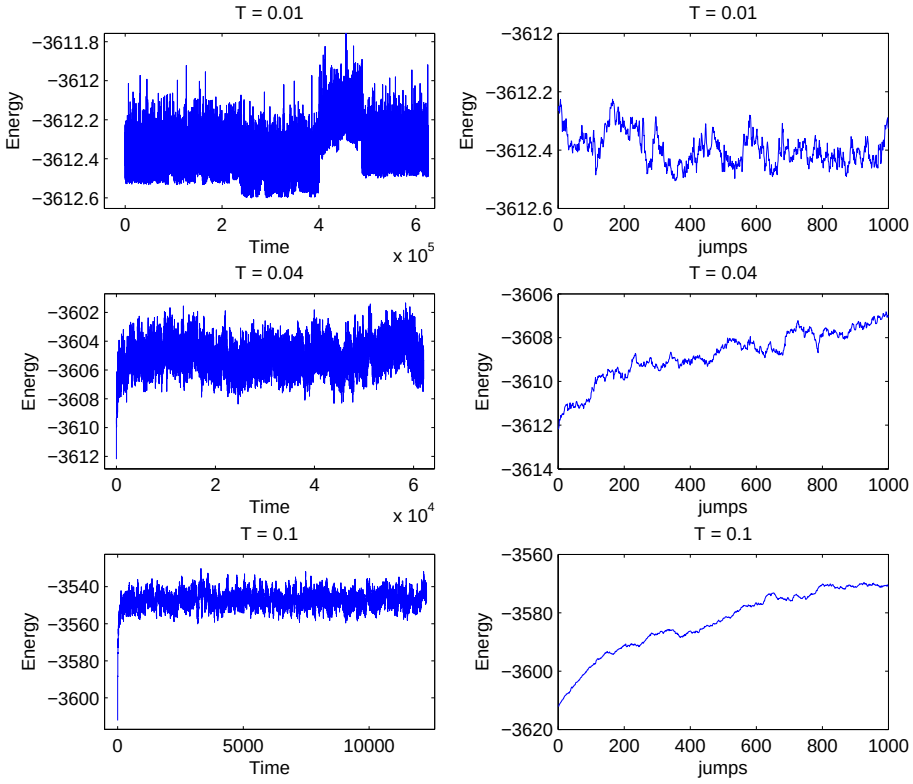

Figure 7.1: Energy evolution for Monte Carlo simulations for three temperatures. All three were started from the same stable initial configuration.

This is particularly evident at low temperatures, as illustrated in figure 7. Here we see that at $T = 0.01$, the system occasionally transfer between low/high energy configurations, while on average remaining stable in energy. These kinds of jumps are less pronounced at higher temperatures.

This behaviour is also illustrated in figure 7.2, where the average occupation probabilities vs. SPE is plotted for four temperatures and fitted to Fermi-Dirac functions. The resulting fitting parameters $(\mu,\ T)$ of the graphs for the four different temperatures shown in figure 7.2 were $(-0.055, 0.0173)$, $(-0.040, 0.027)$, $(-0.022, 0.045)$ and $(-0.015, 0.116)$ respectively.

At temperatures $T = 0.04, 0.1$, the fitting is good, while for the lower temperatures $T = 0.01, 0.02$, the deviation from a pure Fermi-Dirac function must be considered to be large.

In the remainder of part III, for all Monte Carlo results, all averaged quantities were

found by using datasets:

- $T = 0.01$: 6 initial configurations, each 500000 jumps.
- $T = 0.02$: 6 initial configurations, each 500000 jumps.
- $T = 0.04$: 3 initial configurations, each 500000 jumps.
- $T = 0.1$: 1 initial configuration, 500000 jumps.

All systems were allowed to equilibriate by running simulations for large number of before obtaining the jumps used (At T=0.01, and T=0.02: 3 million, at T=0.04 and T=0.1: 1 million).

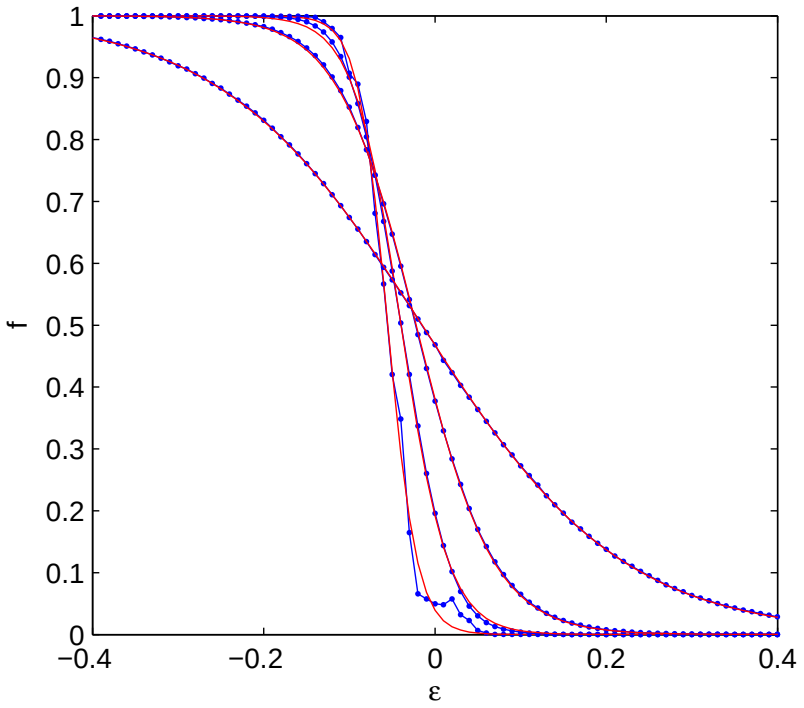

Figure 7.2: Distribution functions at temperatures T=0.01,0.02,0.04,0.1. Dotted blue lines: Occupation probabilities obtained from Monte Carlo simulations. Red lines: Fitted Fermi-Dirac distribution functions. Averaged over 500000 jumps each for 6,6,3 and 1 different initial configurations respectively.

8 Occupation Numbers

We start by investigating the properties of occupation numbers, f_i, and single particle energies, ϵ_i.

The mean field results of these are simply solutions of the self-consistent set of equations, (4.2):

$$\left\{ \epsilon_i = \phi_i + \sum_{j \neq i} \frac{f_j - 0.5}{r_{ij}} \right\}, \; i, j \in \{1, 2, ..., N\} \; , \tag{8.1}$$

where $\{f_j\}$ are the occupation numbers, determined by the Fermi-Dirac distribution function.

The Fermi-Dirac-like dependence of occupation numbers on energy, was confirmed in the previous section, in figure 7.2. Still, it is legitimate to ask to what degree the mean field equations are able to approximate the 'correct' results.

At extremely low temperatures, $T \ll |\epsilon_1|, |\epsilon_2|, .., |\epsilon_N|$, the mean field solutions must tend toward some pseudo-stable state, with all occupation numbers close to 0 and 1. Increasing the temperature, transitions occur with increasing frequency, leading to, on average, a partial charge $\langle n_i \rangle$ on each site. The question we ask is how well the mean field occupations f_i approximate $\langle n_i \rangle$.

We obtain the density of sites with averaged occupation numbers from Monte Carlo simulations. This is done for three temperatures, T = 0.02, T = 0.04 and T = 0.1. The corresponding density of occupation numbers from mean field are found by averaging over 100 solutions for each temperature.

Figure 8.1 shows that the density of sites with occupation numbers $|n_i - 0.5|$, $|f_i - 0.5|$ falls rapidly for values less than 0.5. This fall-off is steeper in the mean field results, and the fraction of sites with occupation numbers different from 0 and 1 is consistently lower compared than the Monte Carlo results.

Then, can we explain why this is? Below, we consider a simple case to argue why the mean field equations are bound to give this behaviour.

Assuming we have a system, consisting of only a single pair of sites sharing one electron, the occupation probability must fulfill detailed balance:

$$\langle n_i \rangle \Gamma_{ij} = \langle n_j \rangle \Gamma_{ji} \; , \tag{8.2}$$

such that

$$\frac{\langle n_i \rangle}{\langle n_j \rangle} = \frac{\Gamma_{ji}}{\Gamma_{ij}} = e^{(\phi_j - \phi_i)/T} \; , \tag{8.3}$$

where ϕ_i, ϕ_j are the on-site energies.

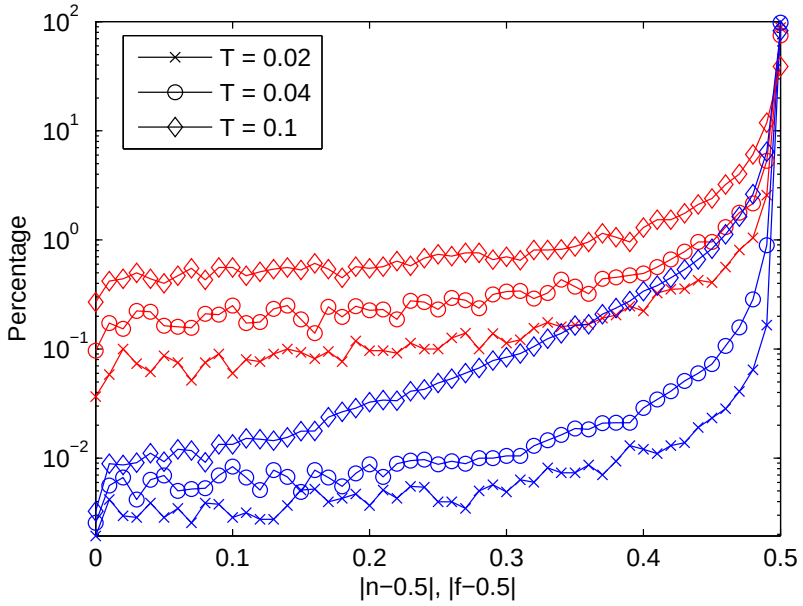

Figure 8.1: Density of sites with $|occupation\ number - 0.5|$. Blue lines: Mean field solutions, averaged over 100 solutions for each temperature. Red lines: Monte Carlo $\langle n_i \rangle$, averaged over $5 \cdot 10^5$ jumps.

Furthermore, since $\langle n_j \rangle = 1 - \langle n_i \rangle$, we get

$$\langle n_i \rangle = \frac{1}{e^{\frac{\phi_i - \phi_j}{T}} + 1} = f_{FD}(\phi_j - \phi_i) \tag{8.4}$$

When the sites are separated by a distance r, the single particle energies are, for the two possible configurations (n_i, n_j),

$$(\epsilon_i, \epsilon_j) = \begin{cases} (\phi_i, \phi_j - 0.5/r), & (n_i, n_j) = (1, 0) \\ (\phi_i - 0.5/r, \phi_i), & (n_i, n_j) = (0, 1) \ , \end{cases} \tag{8.5}$$

depending on where the electron is located.

In the mean field equations, for the same pair of sites, the occupation probabilities are a solution of

$$(f_i, f_j) : \begin{cases} \epsilon_i = \phi_j + (f_j - 0.5)/r \\ \epsilon_j = \phi_i + (f_i - 0.5)/r \end{cases} \tag{8.6}$$

f_i, f_j forms a pair of coupled equations which must be solved numerically. Thus, in contrast to equation 8.4, mean field theory gives

$$f_i = f\big(\phi_i + (f_j - 0.5)/r\big) \tag{8.7}$$

For close pairs, $1/r \sim \phi_i$, this obviously must have consequences.

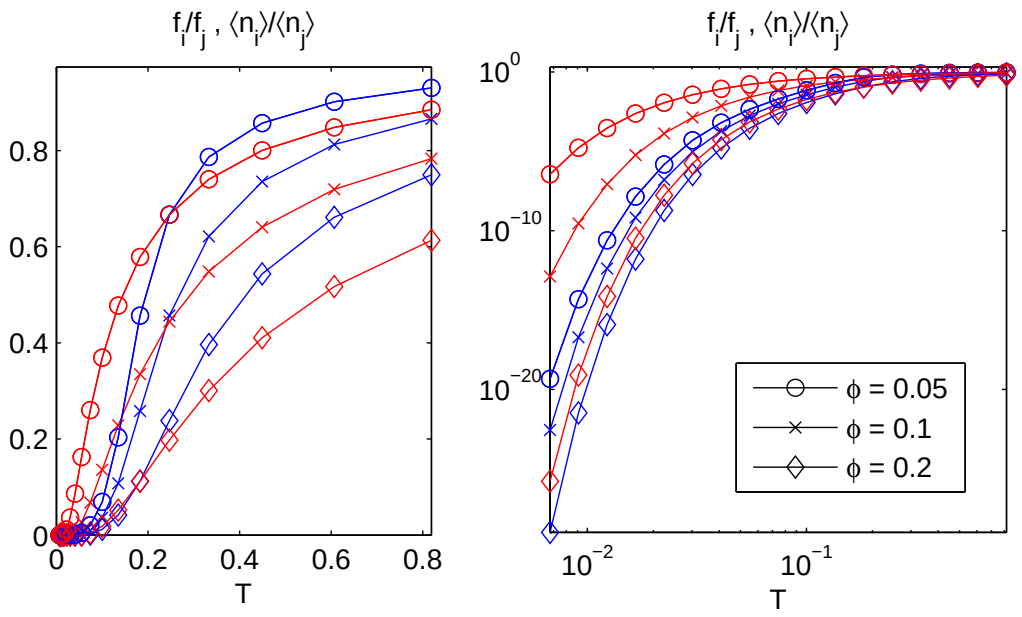

Figure 8.2: Left: Occupation probabilities in a two site-system versus temperature, with $\phi_i = \phi, \phi_j = -\phi$. Red lines: Analytical solution $\langle n_i \rangle / \langle n_j \rangle$ given by (8.2): $e^{-2\phi/T}$ Blue lines: Mean field solution f_j/f_i. Right: Same as left, in logaritmic axes.

In figure 8.2, using $\phi_j = -\phi_i$, $\phi_i = \phi > 0$, it is clear that the mean field results significantly over/underestimates the occupation numbers. At the lower temperatures, f_i, f_j stay close to 0 and 1. Thus, at these temperatures, the solutions are

$$\begin{aligned} f_i &\approx f(\phi + 0.5/r) \\ f_j &\approx f(-\phi - 0.5/r) \end{aligned} \tag{8.8}$$

At the highest temperatures, the opposite effect occurs. Here, both occupation numbers are close to 0.5, and thus, the occupation numbers are given by approximately

$$\begin{aligned} f_i &\approx f(\phi) \\ f_j &\approx f(-\phi) \end{aligned} \tag{8.9}$$

9 Density of States

An important criterion for the validity of the mean-field equations, are their ability to reproduce the correct single particle energy (from hereon SPE) density of states near the Fermi level. This is because these levels, that is, levels close to the Fermi level, are dominating in electronic transitions. Outside this range, sites are with high probability either permanently filled or unfilled.

To check the extent to which this is true, we evolve a system, using a Monte Carlo simulation, starting with initial configurations that have reached thermal equilibrium. The average distribution of SPEs is found by averaging over time. At low temperatures especially, transitions between different pseudo-stable states are very slow. Therefore, we average once more over different initial configurations.

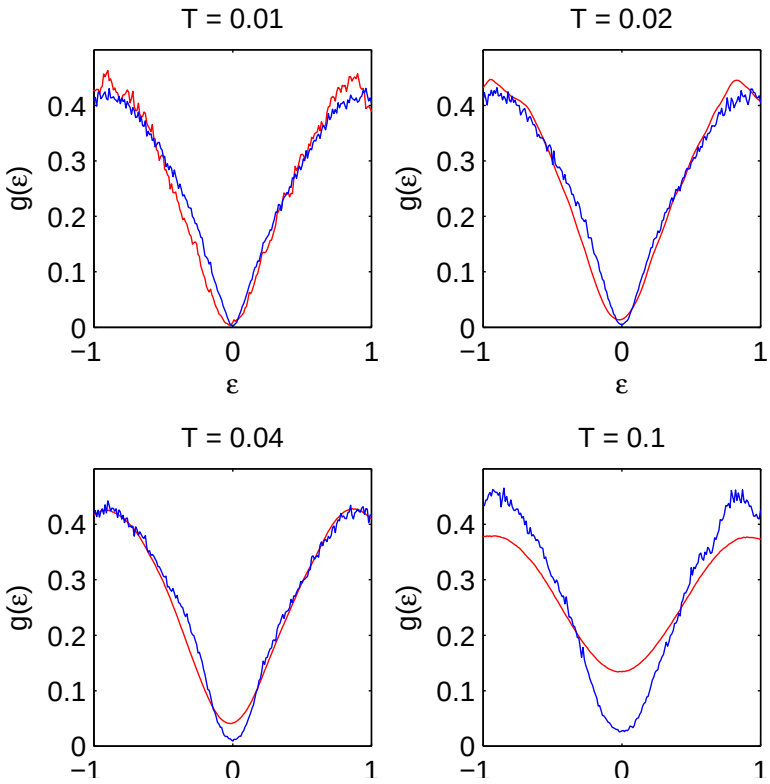

Figure 9.1: The density of states of SPEs at four temperatures: Red lines: Averaged Monte Carlo simulations. Blue lines: Averaged mean field solutions. For Monte Carlo simulations: Averaging were done over one (T=0.1), three (T=0.04), six (T=0.02) and six (T=0.01) Monte Carlo simulations. Mean field solutions were averaged over 100 solutions for each temperature.

The results for the SPE density of states for four temperatures is shown in figure 9.1. At low temperatures (T = 0.01), the curves appearently are very similar. This is expected, since the occupation numbers $\{f_i\}$ are either 0 and 1 with overwhelming probability. At increased temperatures, however, the discrepancy between the two models becomes clearer.

The smearing of the Coulomb gap increasing temperatures is faster in the Monte Carlo simulations, than in the mean-field equations. This is particularly evident at T = 0.1, where the linearity of the Coulomb gap has almost vanished due to thermal effects, while still close to linear in the mean-field equations. These results indicate that the mean-field equations somehow underestimate thermal effects, consistent with the results in the previous section.

On the other hand, at all four temperatures, there are energies in the Coulomb gap where the mean-field equations yield a higher density of states. At T=0.04, this is true from approximately $0.1 < |\epsilon| < 0.5$, and at T=0.01 approximately from $0.0 < |\epsilon| < 0.5$.

These effects can also be seen by plotting the average number of filled states per unit square: $N(\epsilon) = g(\epsilon)f(\epsilon)$, as seen in figure 9.3.

The linear relationship $g(\epsilon) = \alpha|\epsilon|$ of the density of states has been confirmed before for both mean field theory and Monte Carlo methods. In [13], using a Monte Carlo approach to minimize energy, α was found to be consistent with a theoretical prediction of $2/\pi$ in 2D.
In these results, at T = 0.01, a linear fit close to the Fermi level, seen in figure 9.2, gives $\alpha \approx 0.66$ for Monte Carlo simulations, while the mean field results give $\alpha \approx 0.70$. Thus, the Monte Carlo result is closer to the theoretical prediction of $\alpha = 2/\pi \approx 0.64$,

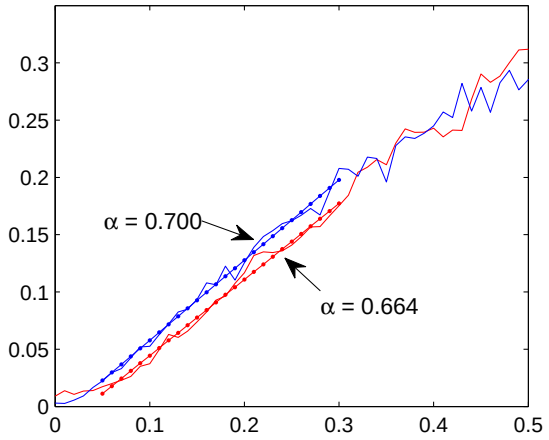

Figure 9.2: Density of states close to the Fermi level at T=0.01, and fitted lines $g = \alpha|\epsilon|$.

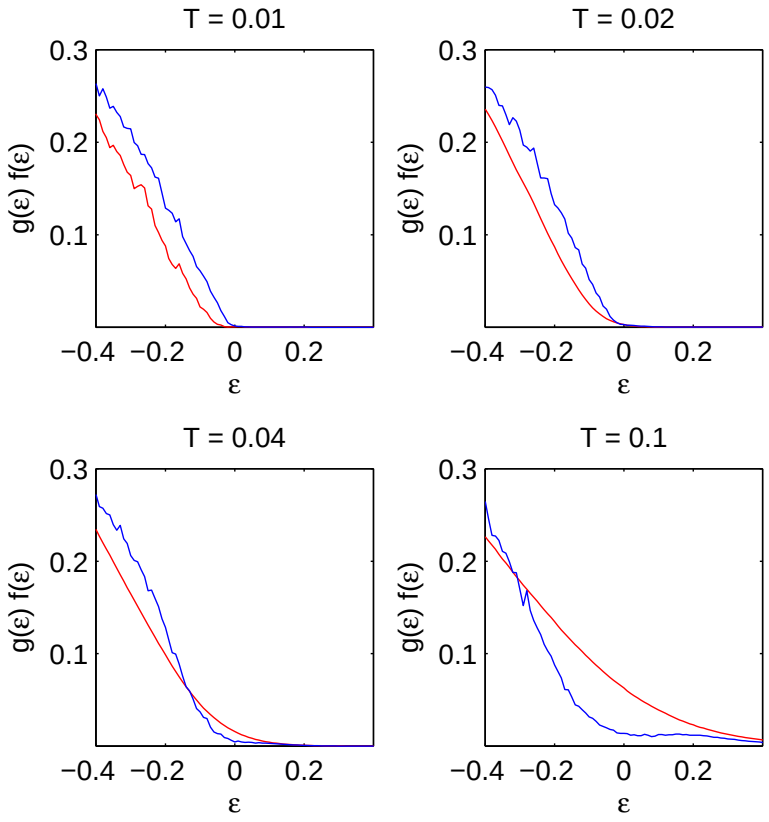

Figure 9.3: Density of states times occupation probability. Red lines: Monte Carlo simulations. Blue lines: Mean field solutions.

Another interesting quantity is the density of states at the Fermi level, $g(0)$. Theoretically, at T=0, $g(0) = 0$. At non-zero temperatures, exitations caused by thermal fluctuations will result in smearing of the Coulomb gap. In [1], using the mean field equations, at a disorder bandwidth $W = 5$, it was found that $g(0)$ increased linearly with temperature: $g(0) = \alpha T$, with $\alpha = 0.15$. Furthermore, this was used as to argue, since α was a small number, that the smearing of the Coulomb gap was a less important element in the shape of the Mott-ES crossover.
Using Monte Carlo methods, in [14], it was found for that for $W = 1$,

$$g(0) = 1.3\ T \tag{9.1}$$

However, according to [15], $g(0)$ depends on W. For $W = 0$, their calculations in [15] found

$$g(0) = 0.85 \exp[-0.3\sqrt{\nu(1-\nu)}/T]\ , \tag{9.2}$$

where $\nu = 1 - K$ is the filling factor. At T = 0.1, for $\nu = 0.5$, this gives the slope of $g'(0.1) \approx 2.8$.

At $W = \infty$, the result was

$$g(0) = 0.085/s + 0.86T \tag{9.3}$$

where s is a factor in the added potential $V(r) = 1/r - 1/\sqrt{r^2 + 4s^2}$, which takes into account screening of Coulomb interaction by a δ-doped layer, or by a gate.

Thus, $g(0)$ should be limited by $\alpha = 0.86$ and $\alpha = 2.8$.

In our model, we consistently use a bandwidth of $W = 1$. Nevertheless, it is interesting to see if we can reproduce a dependence on W for $g(0)$ from the mean field equations.

From figure 9.4, it is clear that the mean field equations significantly underestimates $g(0)$. For the Monte Carlo results, the slope from $T = 0.04$ to $T = 0.1$ is $\alpha \approx 1.54$, which is not to far from the result found in [14].

For the mean field results, $\alpha \approx 0.25$ for both for $W = 5$ and $W = 1$. For these values of W, there is no appearent dependence of $g(0)$ on W.

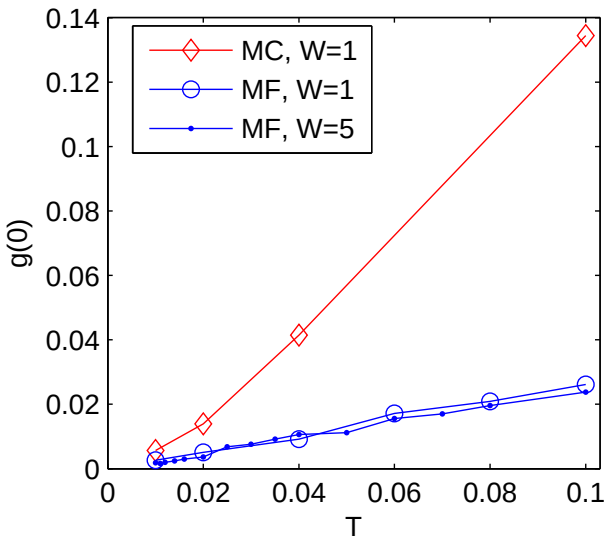

Figure 9.4: Density of states at the Fermi level, $g(0)$. Mean field solutions have been averaged over 100 ($W = 1$) and 50 ($W = 5$). Graphs show a near linear dependence on temperature for mean field equations, while Monte Carlo solutions are near linear at higher temperatures, while showing non-linear behaviour at low temperatures.

10 Transition Rates

In section 3.5.3, we saw that the equations for the mean field transition rates could be reformulated to include correlations in a better way, specifically in order to exlude self-interaction in jumps across the Fermi level.

While these rates certainly yields a better estimate for close pairs, in a large system, the total significance depends on the average spacing between such states.

We will now attempt to make a statistical evaluation of the transition rates to compare the unmodified and modified mean field transition rates to Monte Carlo transition rates.

In the following, we define a quantity which we shall call the 'averaged transition rate': $\langle \sum \Gamma_{E,E'} \rangle$, which tells the average number of jumps per time unit, in the entire lattice, from energies E to E'.

In order to relate these rates to the density of states, $g(\epsilon)$, the energies E, E' are the energies *before* the transition.

10.1 Monte Carlo transitions

In real transitions, jumps only occur from filled sites i to unfilled states j. Thus, the single particle energy at i, on the condition that j is unoccupied, we will label E:

$$E_i = \phi_i + \sum_{k \neq i,j} \frac{n_k}{r_{ki}} \tag{10.1}$$

while for the site site j, the single particle energy, on the condition that there is an electron at site i, we will label E':

$$E'_j = \phi_j + \sum_{k \neq i,j} \frac{n_k}{r_{kj}} + \frac{1}{r_{ij}} \tag{10.2}$$

We study transition rates from $E \to E'$, where E, E' are the single particle energy *before* the transition takes place. The change in energy is then $\Delta\epsilon = E' - E - 1/r$. The transition rate for such a pair, we already know. It is given by equation (4.3).

$\langle \sum \Gamma_{E,E'} \rangle$, on the other hand, depends on the availability of the transitions. This availability, due to correlations, is dependent of the distance between sites. For a sample in a given configuration, at a given distance, r, this availability is found by counting all occupied sites with energy E at a distance r from an unoccupied state E':

$$N(E, E'|r) = \sum_{\left\{ \begin{smallmatrix} i,j,where \\ r_{ij}=r \\ E_i=E, E_i=E' \end{smallmatrix} \right\}} n_i(1 - n_j) \tag{10.3}$$

Averaged over time $t = \sum_n \Delta t_n$, this becomes:

$$\langle N(E, E'|r) \rangle = \frac{1}{\sum_n \Delta t_n} \sum_i \Delta t_n \; N(E, E'|r) \tag{10.4}$$

Now, defining the average transition rates in the Monte Carlo picture,

$$\langle \sum \Gamma_{E,E'} \rangle_{MC} = \int d^2r \; |\Delta\epsilon| \left[N_{BE}(\Delta\epsilon) + \Theta(-\Delta\epsilon) \right] \times \left\langle N(E, E'|r) \right\rangle e^{-2r/a} \tag{10.5}$$

$\langle \sum \Gamma_{E,E'} \rangle_{MC}$ must be evaluated numerically using data from Monte Carlo simulations.

The energies $E,\ E'$ are split into discrete levels, with spacing δE, such that energies in the interval $E \in (E_i - \delta E_i/2, E + \delta E/2)$ were counted as E_i. We use $\delta E = 0.01$ in our calculations.

Due to the even lattice spacing, the space integral becomes a sum over distances, which is cut after a maximum radius of 5: $r_m = \{1,\ \sqrt{2},\ 2,\ \sqrt{5},\ ...,\ 5\}$. This cut was necessary to decrease computation time. Due to the exponential decay of transition rates with r, ($\Gamma_{ij} \propto e^{-2r_{ij}/a}$), transitions at longer distances are insignificant in this context.

Then, numerically, equation (10.5) is calculated as:

$$\left\langle \sum \Gamma_{E,E'} \right\rangle_{MC} = \sum_{\{r_m\}} \langle N(E, E'|r) \rangle |\Delta\epsilon| \left[N_{BE}(\Delta\epsilon) + \Theta(-\Delta\epsilon) \right] e^{-2r_m/a} \tag{10.6}$$

10.2 Mean field transition rates (modified)

The same quantities can be calculated for the modified transition rates defined by equation (4.5), where self-interaction is excluded:

$$\gamma_{ij,mod} = |\Delta\Phi_{ij}| \frac{e^{-\Phi_{i(j)}/T}}{Z_{ij}} e^{-2r_{ij}/a} [N_{BE}(|\Delta\Phi_{ij}|) + \Theta(-\Delta\Phi_{ij})] \tag{10.7}$$

where Z_{ij} is given by equation (3.43) and $\Delta\Phi_{ij} = \Phi_{i(j)} - \Phi_{j(i)}$.

The solutions to the mean field equations give sets $\{\epsilon_1, \epsilon_2, ..., \epsilon_N\}$, and corresponding occuption numbers $\{f_1, f_2, ..., f_N\}$. Since the modified mean field rates depend, rather than on ϵ, on the quantities Φ, a calculation of $\langle \sum \gamma_{\epsilon,\epsilon'} \rangle_{MF,mod}$ requires that ϵ's are substituted by Φ's in the following way, for two sites i, j:

$$\Phi_{i(j)} = \epsilon_i - \frac{f(\epsilon_j)}{r_{ij}} \tag{10.8}$$

$$\Phi_{j(i)} = \epsilon_j - \frac{f(\epsilon_i)}{r_{ij}} \tag{10.9}$$

such that the energy difference in a transition $i \to j$ is given by:

$$\Delta\Phi_{ij}(r_{ij}) = \Delta\Phi(\epsilon_i, \epsilon_j, r_{ij}) = \epsilon_j - \frac{f(\epsilon_i)}{r_{ij}} - \epsilon_i + \frac{f(\epsilon_j)}{r_{ij}} \tag{10.10}$$

As in section 10.1, we can define the energies E and E', which are the single particle energies, at site i and j respectively, *before* the jump:

$$\begin{aligned} E &= \Phi_{i(j)} \\ E' &= \Phi_{j(i)} + \frac{1}{r_{ij}} \end{aligned} \tag{10.11}$$

Then the sum of all transition rates from energies E to E' are, for one solution S:

$$\begin{aligned} \left(\sum \gamma_{E,E'}\right)_{MF,mod,S} = \sum_{\{r_m\}} \sum_{\left\{\begin{smallmatrix} i,j,where \\ r_{ij}=r_m, \\ \Phi_{i(j)}=E, \\ \Phi_{j(i)}=E'-1/r_{ij} \end{smallmatrix}\right\}} & \frac{e^{-\Phi_{i(j)}/T}}{Z_{ij}} |\Delta\Phi_{ij}(r_m)| \times \\ & [N_{BE}(\Delta\Phi_{ij}(r_m)) + \Theta(-\Delta\Phi_{ij}(r_m)] \ e^{-2r_m/a} \end{aligned} \tag{10.12}$$

We then assume that the average of equation (10.12) is given by the average over many solutions:

$$\left\langle \sum \gamma_{E,E'} \right\rangle_{MF,mod} = \frac{1}{N_S} \sum_{S=1}^{N_S} (\sum \gamma_{E,E'})_{MF,mod,S} \tag{10.13}$$

10.3 Mean field transition rates (unmodified)

Likewise, the mean field transition rates defined by equation (3.21), can be associated with a a set of corresponding 'averaged transition rates' from sites of energies ϵ to ϵ':

$$\left\langle \sum \gamma_{\epsilon,\epsilon'} \right\rangle_{MF} = |\Delta\epsilon| \times [N_{BE}(\Delta\epsilon) + \Theta(-\Delta\epsilon)] \int d^2r \ \langle N(\epsilon, \epsilon'|r)\rangle e^{-2r/a} \tag{10.14}$$

where $\Delta\epsilon = \epsilon' - \epsilon$. Now, since the occupation numbers only depends on Fermi functions $f(\epsilon)$, $N(\epsilon, \epsilon'|r)$ is, for a given solution:

$$N(\epsilon, \epsilon'|r) = \sum_{\left\{\begin{smallmatrix} i,j,where \\ r_{ij}=r_m \\ E_i=E, E_j=E' \end{smallmatrix}\right\}} f(\epsilon_i)(1 - f(\epsilon_j) \tag{10.15}$$

Again, with even lattice spacing, for a solution S, the sum of all transitions from energy ϵ to ϵ' is calculated numerically as:

$$\left(\sum \gamma_{\epsilon,\epsilon'}\right)_{MF,S} = \sum_{\{r_m\}} \sum_{\left\{\begin{smallmatrix} i,j,where \\ r_{ij}=r_m \\ \epsilon_i=\epsilon, \epsilon_j=\epsilon' \end{smallmatrix}\right\}} f(\epsilon_i)(1 - f(\epsilon_j)|\Delta\epsilon_{ij}| \left[N_{BE}(\Delta\epsilon_{ij}) + \Theta(-\Delta\epsilon_{ij})\right] \ e^{-2r_m/a} \tag{10.16}$$

and the average:

$$\left\langle \sum \gamma_{E,E'} \right\rangle_{MF,S} = \frac{1}{N_S} \sum_{S=1}^{N_S} \left(\sum \gamma_{E,E'} \right)_{MF,S} \tag{10.17}$$

The energies, ϵ, in (10.16) are of a different character than the E's in equations (10.12) and (10.6), which are always from an occupied to an unoccupied site. Rather, the ϵ's in (10.16) are the energies in *partially* occupied sites.

However, it is possible to do an adjustment like that in section 10.2: For each distance r_m, the energies ϵ and ϵ' are substituted by:

$$\begin{aligned} \epsilon(r_m) = \Phi_{\epsilon(\epsilon')} + \frac{f(\epsilon')}{r_m} \rightarrow E = \Phi_{\epsilon(\epsilon')} = \epsilon(r_m) - \frac{f(\epsilon')}{r_m} \\ \epsilon'(r_m) = \Phi_{\epsilon'(\epsilon)} + \frac{f(\epsilon')}{r_m} \rightarrow E = \Phi_{\epsilon'(\epsilon)} + \frac{1}{r_m} = \epsilon' + \frac{1 - f(\epsilon)}{r_m} \end{aligned} \tag{10.18}$$

The effect of this substitution is illustrated in figure 10.1.

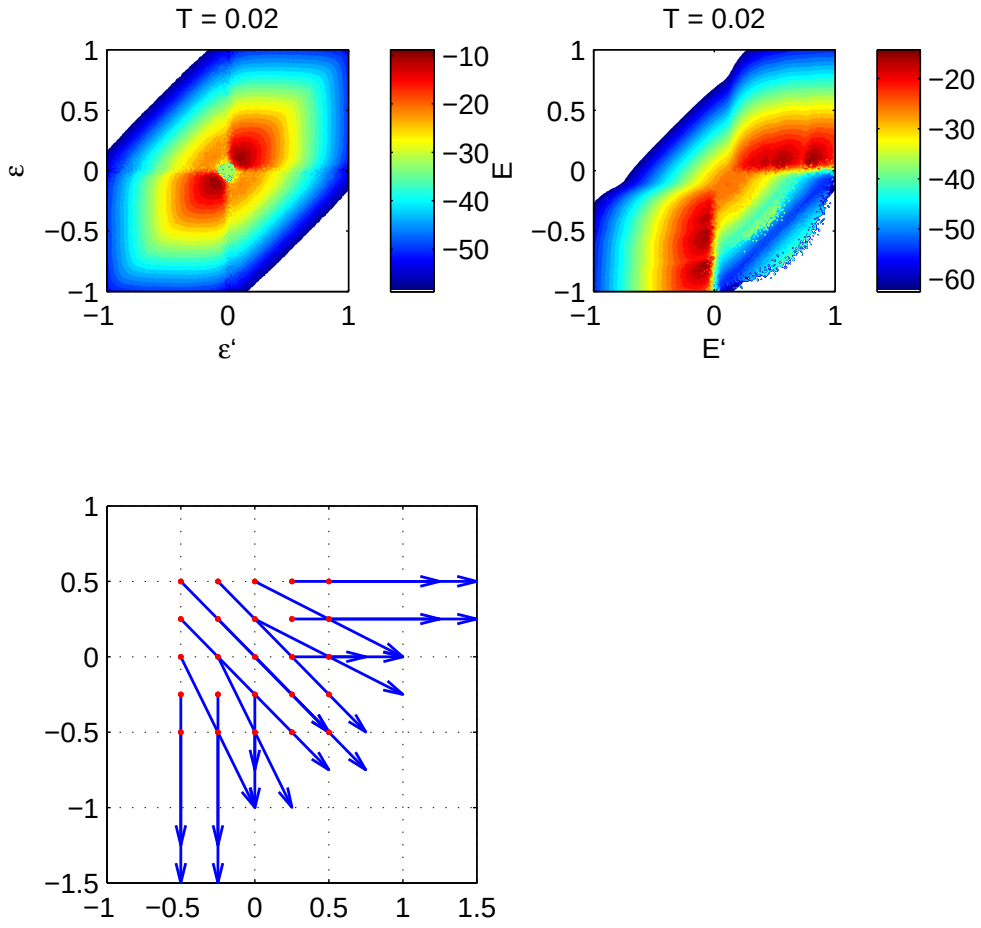

Figure 10.1: Going from energies ϵ to E at $T = 0.02$. Upper left: Transition rates for unmodified equations, with the original site energies ϵ and ϵ'. Upper right: The same rates with energies adjusted according to (10.18. Colors determined by value of $log(\langle\gamma\rangle)$.
Bottom left: Vectors showing the change at $T = 0.02$ and $r_m = 2$. Arrows: Vectors showing the change $(E, E') - (\epsilon, \epsilon')$, where red dots are placed in (ϵ, ϵ').

10.4 Results and Discussion

The averaged transition rates were computed numerically for mean field and Monte Carlo solutions at three temperatures: T = 0.02, 0.04, 0.1.

For mean field solutions, the results were obtained by averaging over $N_S = 100$ solutions.

The Monte Carlo results were averaged using six (T=0.02), three (T=0.04) and one (T=0.1) different initial configurations and averaging over 20000 jumps each.

In all plots in figure 10.3 and 10.4, the effect of regularity of the lattice is clear. At $T = 0.02$, transitions are most frequent along thin 'strips' along $E = E' - 1/r_m$, $(r_m = 1, \sqrt{2}, 2, ...)$. These strips are smeared at higher temperatures.

Comparing the Monte Carlo (figure 10.3) and mean field results (figure 10.4) for the transition rates, we see that at $T = 0.02$, the modified mean field equations strongly resemble the rates from Monte Carlo simulations, with a clear preference for jumps across the Fermi level along the strips.

At $T = 0.1$, jumps seem to be concentrated in an ellipse centered around$(E, E') = (-0.5, 0.5)$ in the Monte Carlo results. This shape is similar, but distorted in the modified mean field result.

From the plots of the unmodified mean field transition rates, shown in the right hand side plots in figure 10.4, it is clear that this form of expression of the transition rates, especially at low temperatures, in practice leads to eliminating the bulk of all probable transitions, the jumps across the Fermi level.

Instead, at temperatures T=0.02 and T=0.04, the large majority of jumps are between sites on the same side of the Fermi level. Only for the highest values of r_m are the transition rates across the Fermi level reasonably large, while in practice absent for nearest neighbors. At the highest temperature, this tendency is still present, but weaker.

We have now shown that the mean field transition rates, in the unmodified form, in this temperature range, are unable to give a realistic result compared to Monte Carlo simulations.

In the coming sections, we do conductivity calculations, using resistor networks. It then is important to know if any differences, compared to Monte Carlo results, can be explained simply by the discrepancy between mean field and Monte Carlo transition rates.

In this respect, an important quantity is the *total* transition rate. For Monte Carlo:

$$\Gamma_{tot} = \sum_{i,j} \Gamma_{ij} \tag{10.19}$$

and for mean field:

$$\gamma_{tot} = \sum_{i,j} \gamma_{ij} \tag{10.20}$$

The averages of these must be the sum over E, E' in the maps in figure 10.3 and 10.4.

For Monte Carlo data, this is equivalent to:

$$\langle \Gamma_{tot} \rangle = \frac{\#jumps}{T_{tot}} \tag{10.21}$$

where $\#jumps$ is the number of jumps during a time T_{tot}.

As figure 10.2 shows, the *total* modified mean field transition rates closely follows the total Monte Carlo rates. Curiously, the difference is largest at T=0.02, where the mean field result is about two times larger than the Monte Carlo result. This fact may be partially explained by the overestimation of the density of states near the Fermi level in the mean field results.

Furthermore, we look at how the jump length of transitions. Defining:

$$\sum \Gamma(r) = \sum_{\left\{ \substack{i,j,where \\ r_{ij}=r} \right\}} \Gamma_{ij} \tag{10.22}$$

In figure 10.5, the fraction of all transitions for a given jump length is plotted, showing that at the lowest temperature, T=0.02, the Monte Carlo and the modified mean field transition rates yield roughly the same result. For higher temperatures, the tendency is toward a higher preference for longer jumps in the Monte Carlo results than for mean field results. Again, as would be expected, the unmodified mean field results are in strong disagreement with the other results.

In terms of absolute values, for the modified mean field rates, the relative error $\left(\left(\sum \gamma(r)_{mod} - \sum \Gamma(r) \right) / \sum \Gamma(r) \right.$ shows the same tendency. For T=0.02, the relative error is about 1 for all jump lengths. At the higher temperatures, the error is consistently shrinking with jump length.

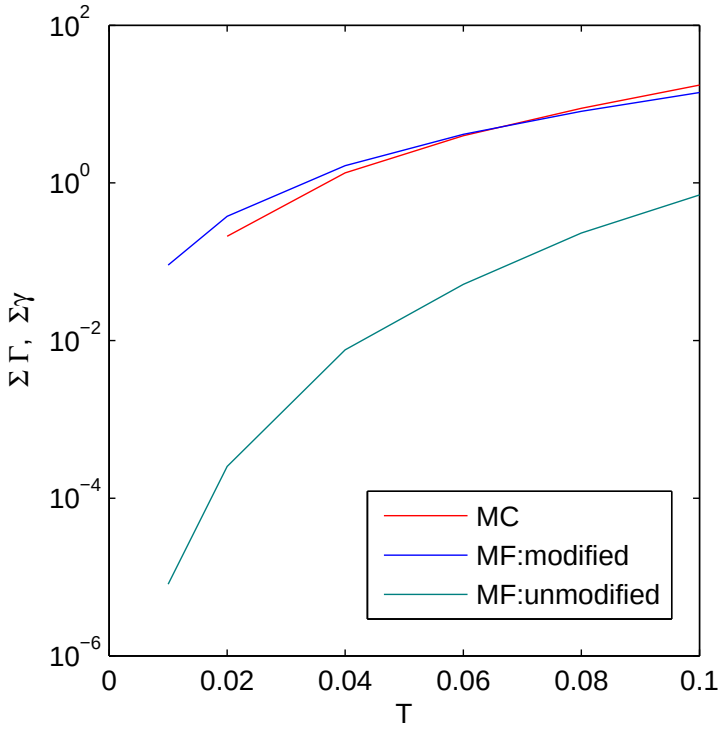

Figure 10.2: The total transition rate, given by $\sum_{ij}\Gamma_{ij}$ and $\sum_{ij}\gamma_{ij}$ for Monte Carlo and mean field results, respectively, in logaritmic y-axis.

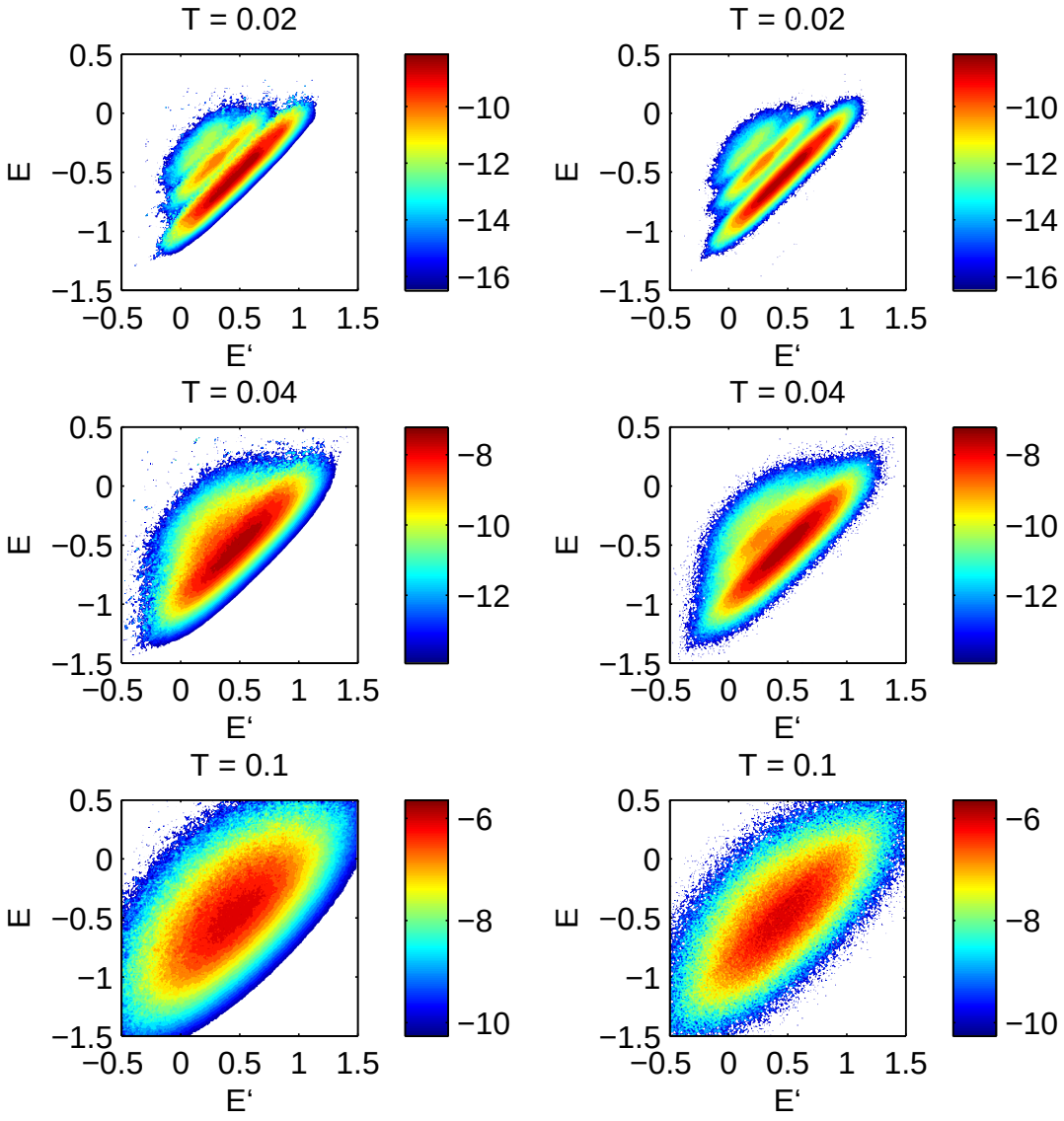

Figure 10.3: Left column: Logaritmn of averaged transition rates $\langle \sum \Gamma_{E,E'} \rangle_{MC}$. Right column: Logarithm of transition rates of all actually performed jumps by the Monte Carlo program. The colors scales are the same for the same temperatures. Values below the lowest color in the colorbar are white.
At low temperatures, there is a very strong preference for jumps across the Fermi level. At higher temperature, this preference is weaker. The regularity of the lattice is appearent: Most jumps are made in a small band around $\epsilon' - \epsilon - 1/r_i$.

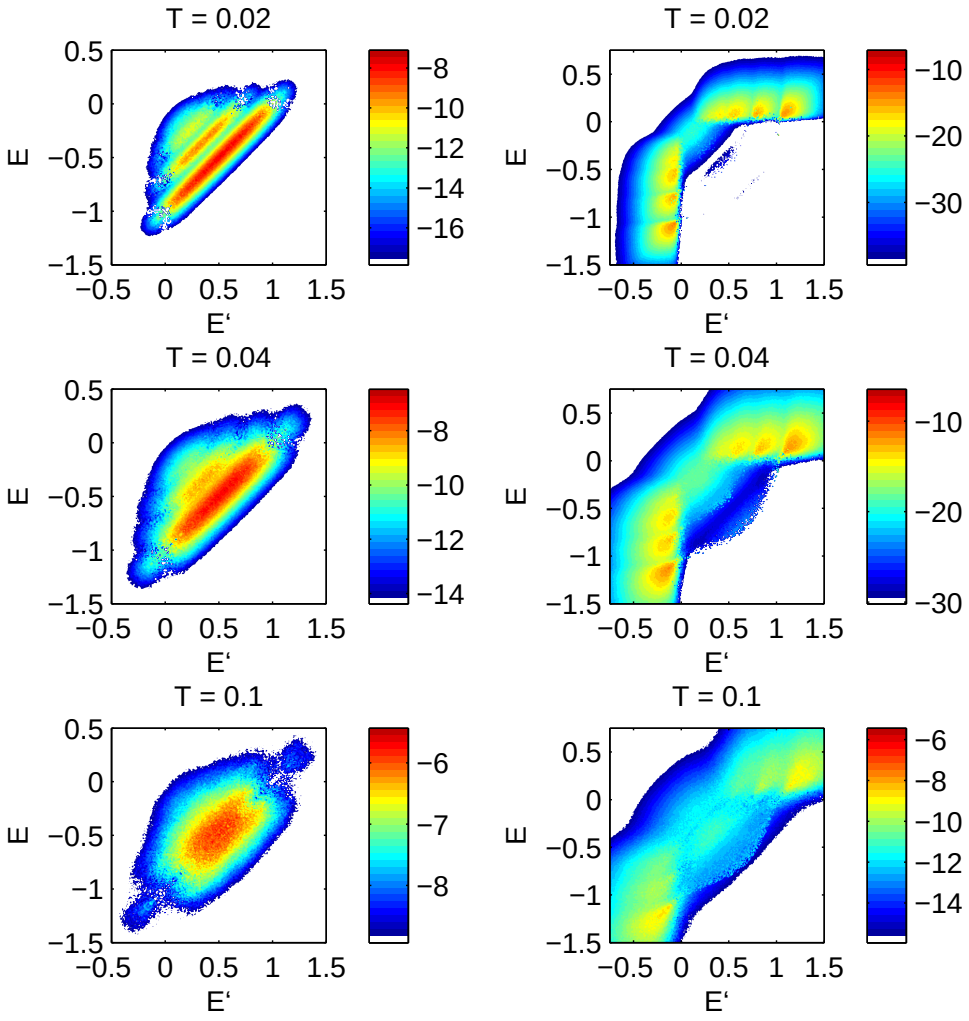

Figure 10.4: The averaged mean field transition rates. Color scaling is the same for same temperatures. Values below minimum in colorbar are white.
Left column: (Logaritmn of) averaged modified transition rates $\langle \sum \Gamma_{E,E'} \rangle_{MF,mod}$.
Right column: (Logaritmn of) averaged unmodified transition rates $\langle \sum \Gamma_{E,E'} \rangle_{MF}$, after the substitution $\epsilon \to E$
Transitions across the Fermi level are nearly blocked for the nearest neighbors in the unmodified transition rates, while the modified strongly resemble those obtained in Monte Carlo simulations, seen in figure 10.3

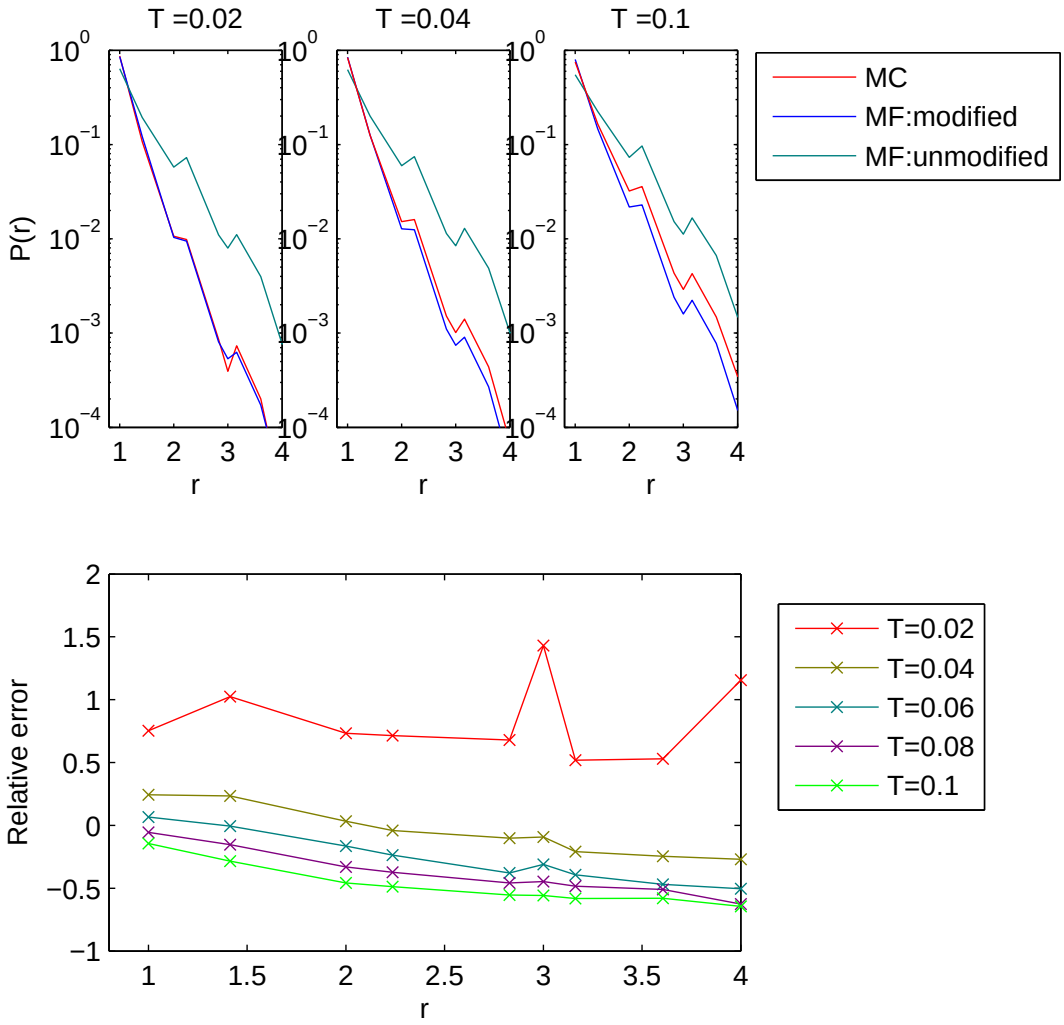

Figure 10.5: Top plots: The fraction of all transition rates with jump length r, $P(r) = \sum \Gamma(r)/\Gamma_{tot}$ for Monte Carlo. $P(r) = \sum \gamma(r)/\gamma_{tot}$, for mean field. Bottom: The relative error in sum of mean field modified transition rates compared to Monte Carlo results: $\big((\sum \gamma(r) - \sum \Gamma(r)\big)/\sum \Gamma(r)$.

Part IV
Current Properties

11 Percolation Thresholds and Size Effects

Mean field theory predicts that the jump length at the percolation threshold increases with lower temperature: $r \propto (1/T)^{1/2}$. The finite size of the lattice, combined with this increase, means that finite size effects must play a larger role at lower temperatures. These effects manifest themselves in the results of conductivity and other properties.

These size effects are related to the variance in the percolation treshold, $Var(\xi_c)$). For an infinite sample, we expect $Var(\xi_c) \to 0$.

We find ξ_c by calculating the conductivity for resistor networks with varying maximal values of resistors. Figure 11.1 show ξ_c for 10 different samples at temperatures $T \in [0.16, 0.1]$, where:

$$\xi_c = -\ln(\tilde{\Gamma}_c) \tag{11.1}$$

Γ_c is the critical resistor. In addition to ξ_c, ξ_1, the ξ-value of the resistor at 99% of maximal current is shown in figure 11.1.

A line fit of ξ_c to the function $y = (c/T)^p$ yields $p = 0.510 \pm 0.007$, $c = 8.6$ for the modified and $p = 0.500 \pm 0.005$, $c = 14.0$ for the unmodified mean field equations.

As a reminder, the derivation in section 3.6.2 used the unmodified form of the resistor network with the result $p = 1/2$. Thus, we have shown that in our model, using the modified version of the resistor network has only a small effect on the value of p.

Thus, we can expect that the Efros-Shklovskii law should be followed in our model in both forms of the resistor networks, but with a different value of T_0.

The variance of ξ_c is shown in figure 11.2. At low temperatures, the variance of ξ_c is consistently higher for the modified network. Referring to figure 11.3, we can perhaps understand why: The strong preference for close jumps seldom form critical connections of clusters. Instead, these transitions contribute to the formation of smaller, isolated clusters.

In figure 11.3, the resistors at and below the percolation limit is drawn, for both the modified and unmodified resistor networks. In the unmodified network, the preference for connections between sites on the same side of the Fermi level is clear, as is also seen in figure 10.4.

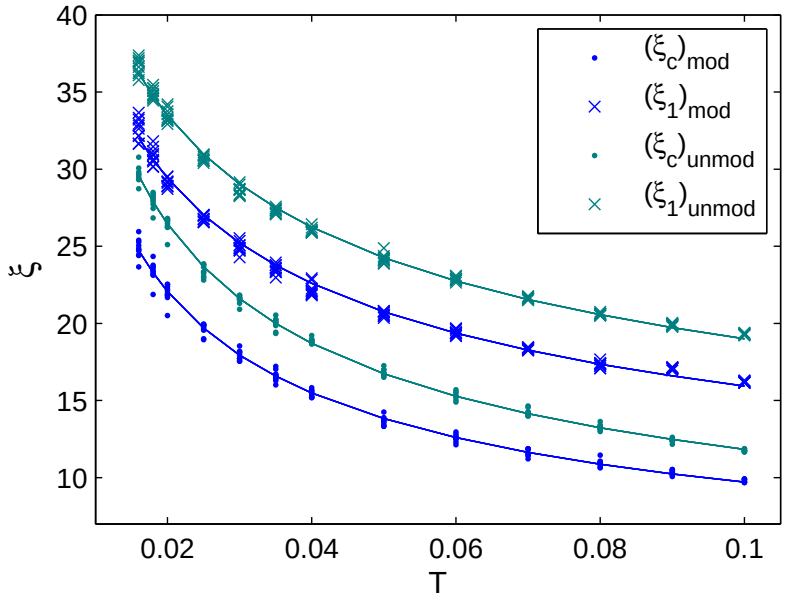

Figure 11.1: Percolation thresholds vs. T and fits to the function $f = (c/T)^p$. ξ_c is the value of the resistance at which the system percolates. ξ_1 is the value of the resistor at which the total calculated current is 99% of the total current. At lower temperatures, there is an increasing spread in values of ξ.

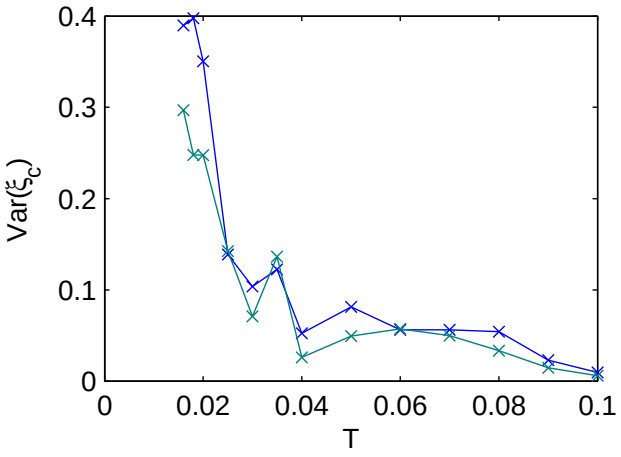

Figure 11.2: The variance of the percolation limit ξ_c, for the modified (blue) and unmodified (green) resistance networks.

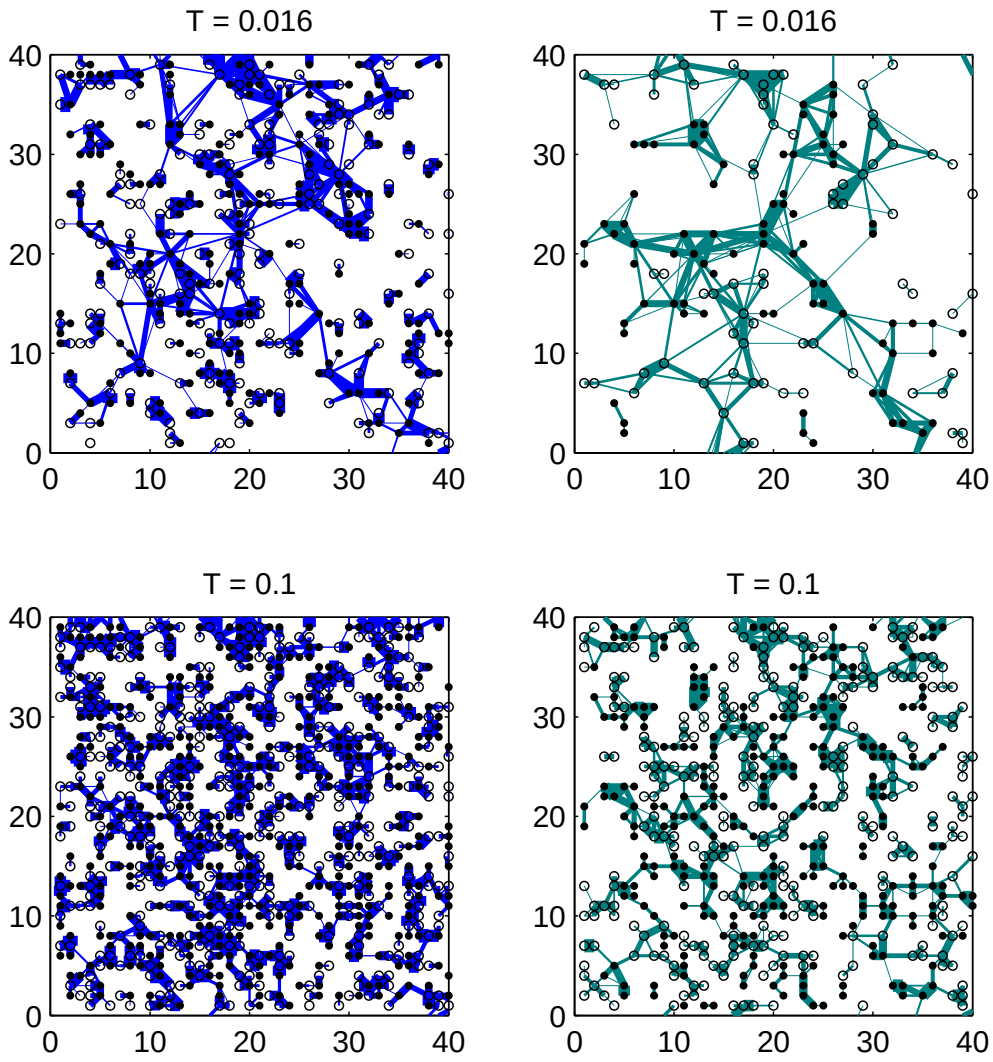

Figure 11.3: Zoom-in on 100x100 resistor networks, all bonds below or at the percolation treshold, with thickness determined as fraction of logaritm of strongest bond. Top plots are at temperature T=0.016. Lower plot are at temperature T=0.1.
Dots/circles: Sites with negative/positive energy connected to a cluster.
Left: Modified resistance network, 3220 (T=0.016) and 7521 (T=0.1) bonds.
Right: Unmodified resistance network, 2030 (T=0.016) and 5146 (T=0.1) bonds.

12 Conductivity

Efros and Shklovskii's law is derived using mean-field theory, and states that the conductivity, at temperatures where a Coulomb gap has been formed, should follow $\sigma = \sigma_0 e^{-(T_0/T)^{1/2}}$. $T_0 = \beta/a$. β is a numerical factor, dependent of dimensionality and a is the localization length. The 1/2-exponent is independent of dimensionality, which follows from the shape of the density of states around the Fermi level: $g(\epsilon) \propto |\epsilon|^{d-1}$.

As shown in the previous section, $e^{-(c/T)^{1/2}}$-dependence of ξ_c was followed for both forms of the resistor networks.

Previous calculations, [11] and [16], have confirmed that for Monte Carlo methods, that the system is in the ES-regime at these temperatures.

We now make calculations of the conductivity using mean field resistor networks and compare to Monte Carlo results in the temperature range $T \in [0.16, 0.1]$.

12.1 Monte Carlo conductivity

Following [11], the conductivity for Monte Carlo results is

$$\sigma = \frac{j}{E_f} = \frac{1}{L^2}\frac{dp}{dt}\frac{1}{E_f} \ , \tag{12.1}$$

where $j = 1/L^2 \frac{dp}{dt}$ is the current density and p is the *accumulated charge*, caused by the net displacement of electrons in the direction of the electric field:

$$p = \sum_{jumps\ n} \Delta x_n \tag{12.2}$$

12.2 Mean field conductivity

Following the prescription in section 6.2, calculations are made for the conductivities of the resistor networks, when the resistors are given by 3.36:

$$R_{ij} = \frac{T}{\gamma_{ij}}$$

The conductivity is again given by $\sigma = j/E_f$, but where the current density now is given by

$$j = J_{tot}/L \tag{12.3}$$

The electric field is, when the potential is V,

$$E_f = V/L \ , \tag{12.4}$$

such that the conductivity

$$\sigma = J_{tot}/V \ . \tag{12.5}$$

12.3 Results and Discussion

We compare the conductivity in the temperatue range $T \in [0.016, 0.1]$, using calculations for both the resistance network of both the modified and unmodified transition rates given by equations (4.4) and (4.5), in addition to results from Monte Carlo simulations [3].

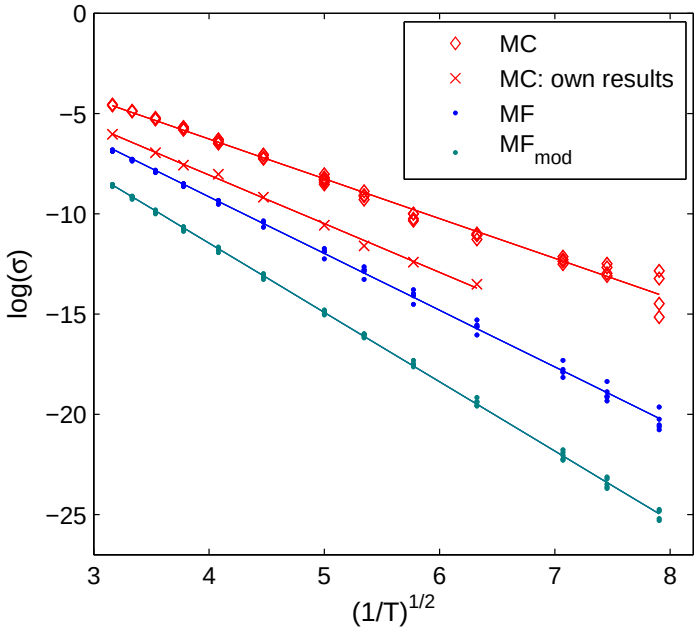

Figure 12.1: Left: Logarithm of conductivity vs. $1/T^{1/2}$, for Monte Carlo and mean field results, as specified in legend. Solid lines show line fits, while markers are results obtained from calculations/simulations.

Expecting Efros-Shklovskii's law, both for mean field and Monte Carlo results, we make plots of the logarithm of conductivity versus $T^{-1/2}$. Figure 12.1 shows that graphs are close to linear for all results, with some deviance in the Monte Carlo results.

Thus, for mean field, both the unmodified and modified resistor networks yield the Efros-Shklovskii law, in line with the results in section 11. The plots in figure 12.2 give further insight as to why: Current is, relative to all transitions (see figure 10.4), disproportionately distributed between states on the same side of the Fermi level, which is in line with the derivation of the Efros-Shklovskii law.

[3] These results are from simulations performed by Joakim Bergli

The Monte Carlo results (labelled *MC*) have been obtained using a different[4] expression for rates than in equation (5.4). Rather, with a cut-off $P_m = 1$:

$$\Gamma^A = \exp\left(\frac{-|\Delta\epsilon|}{T}\right) \tag{12.6}$$

A few results (labelled *MC: own results*) have been included, using the rates given by (5.4) and cut-off rate $P_m = 3$.

Assuming that the conductivity follows the Efros-Shklovskii law, using linear fits, $y = \alpha x$, this give values for β:

$$\beta = T_0 \cdot a = \alpha^2 \tag{12.7}$$

For Monte Carlo results, $\beta = 3.9 \pm 0.23$, while the modified, unmodified mean field results give $\beta = 12.0 \pm 0.05$ and $\beta = 8.0 \pm 0.10$ respectively.

The other Monte Carlo results (*MC: own results*) give $\beta = 5.90 \pm 0.35$, which is closer to the modified mean field results. In addition, the values for σ_0 are closer to the mean field estimation for these results.

These results shows that the unmodified mean field results significantly underestimates conductivity in this temperatures range. This fact can in part be understood by the results from section 10, where it was shown that most transitions are significantly underestimated.

The modified mean field results are in better agreement with the Monte Carlo results, although they also underestimate current for the temperature range.

While this work focuses on the low-temperature properties, as a bonus, figure 12.3 shows what happens at increased temperatures: Modified and unmodified mean conductivity merge with Monte Carlo results.

[4]The choice for Γ^A was made in order to compare results to another research group, and independent of this thesis. The choice can be justified that the exponential tail, combined with non-divergent behaviour at $\Delta\epsilon = 0$ is most important, and since the dependence on the preexponential factor ν_0 varies from model to model ($\propto |\Delta\epsilon|$,$\propto |\Delta\epsilon|^2$,...)

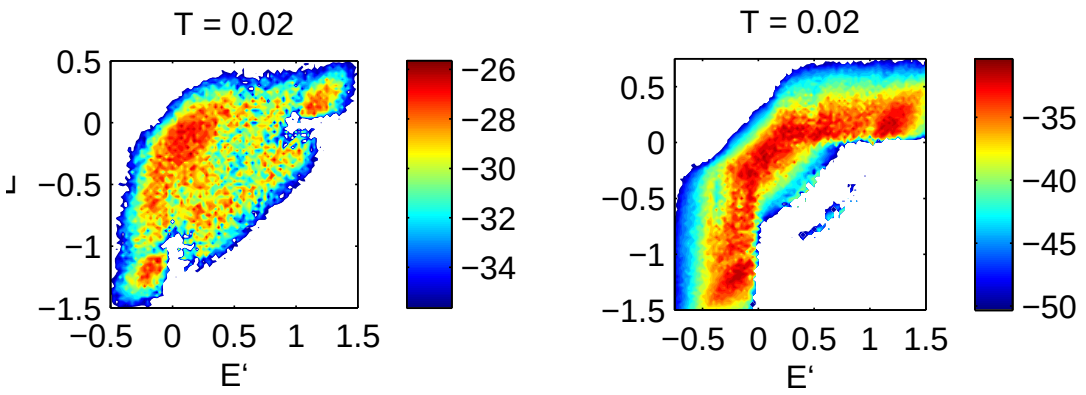

Figure 12.2: Left: (Logarithm of) currents from energies E to E', averaged over 100 solutions. Left: Modified resistor network. Right: Unmodified resistor network.

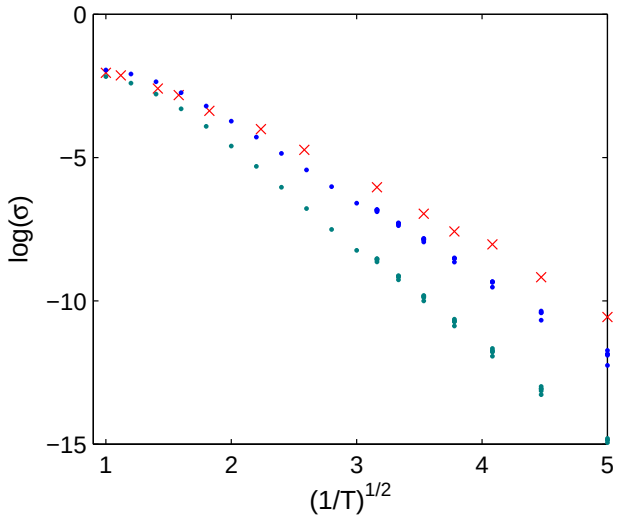

Figure 12.3: Conductivities estimated by mean field and Monte Carlo methods. Markers as in figure 12.1

13 Preliminary Conclusion and Discussion

In part III, we compared equilibrium properties of Coulomb glasses, as estimated by mean field results, to results from Monte Carlo simulations. These were done at temperatures were the Coulomb gap was well established.

In section 10 it was shown that the unmodified form of the transition rates 4.4 significantly underestimated transitions across the Fermi level.

This result had consequences on the results for conductivity in the previous section. The modified resistor network yielded results which were in better agreement with Monte Carlo simulations, while the unmodified network grossly underestimated the conductivity, both compared to Monte Carlo and the modified mean field results.

With these results in mind, for the remainder of this thesis, we focus on the modified version of the mean field transition rates. Thus in the following, all references to mean field results are to the modified resistor networks.

In the next section, we try to explain how the disagreement with Monte Carlo conductivity arise.

14 Hopping Lengths

Until now, we have seen that there is a discrepancy between all results from Monte Carlo and mean field methods. These differences must also manifest themselves in the average jump lengths required to cross the samples.

The mean field estimate for the critical hopping length, equation (3.56), which gave

$$r_c \propto \sqrt{1/T}$$

is derived from the percolation threshold ξ_c. It therefore does not equal the average hopping length, but rather some characteristic length of the resistance network. The *average* jump length should be lower, but of the same form.

We now use mean field and Monte Carlo data to compare hopping lengths.

14.1 Monte Carlo hopping lengths

In the Monte Carlo picture, the definition of the average jump length is a problem in itself, since, in the ohmic regime, transitions are dominated by a massive amount of jumps that does not contribute to current, but rather to noise.

To be able to compare quantities in the mean field picture to Monte Carlo results, we look at two approaches to see if any yield the desired $r \propto \sqrt{1/T}$-behaviour.

14.1.1 I: Net current between sites

One approach to defining currents is as the sum of all (absolute values of) net currents between pairs of sites:

$$N_{ij} = |n_{ij} - n_{ji}| \tag{14.1}$$

where n_{ij}, n_{ji} is the number of jumps from i to j and j to i respectively, such that N_{ij} is the net number of jumps between sites i, j, in the simulation. The average jump length then becomes, using N_{ij} as weights:

$$\langle r \rangle_{I_{(MC)}} = \frac{1}{\sum_{i,j,i>j} N_{ij}} \sum_{i,j,i>j} N_{ij}\ r_{ij} \tag{14.2}$$

14.1.2 II: Net current in direction of electric field

The effect of the electric field is that, on average, there are more jumps in one direction than the other. In our case, since the electric field is in the x-direction, there is an average displacement of electrons in the opposite direction. For each simulation, there is a quantity N_T,

$$N_T(\Delta x) = N(-\Delta x) - N(\Delta x) \tag{14.3}$$

where $N(\Delta x)$ is the total number of jumps with displacement Δx in the x-direction.

Then, for each Δx, there is an average jumplength:

$$\langle r(\Delta x) \rangle = \frac{1}{N(-\Delta x) + N(\Delta x)} \sum_{\left\{ \substack{i,j,where \\ |\Delta x_{ij}| = \Delta x} \right\}} r_{ij} \tag{14.4}$$

We can then define an average jump length:

$$\langle r \rangle_{II_{(MC)}} = \frac{1}{\sum_{\Delta x=1}^{10} N_T(\Delta x)} \sum_{\Delta x}^{10} N_T(\Delta x) \langle r(\Delta x) \rangle \tag{14.5}$$

We find $N_T(\Delta x)$ by summing over data from many different Monte Carlo samples, that is, with different initial configurations and disorder (ϕ -) configuration. This is necessary, since, especially at low temperatures, N_T fluctuates signicantly from sample to sample.

14.2 Mean field hopping lengths

Having found the potentials at each site $\{U_i\}$, the current between a pair of sites i, j is given by:

$$J_{ij} = (U_i - U_j)\tilde{\Gamma}_{ij} \tag{14.6}$$

Then, as in the Monte Carlo picture, we can define two average jump lengths, analogues to the Monte Carlo definitions. The analogue to I_{MC} (section 14.1.1), in the mean field picture is the *true* average jump length. Nonetheless, for comparison, we will also define the analogue to $II_{(MC)}$ (14.1.2).

14.2.1 I: Net current between sites

The mean field analogue to method I is

$$\langle r \rangle_{I_{(MF)}} = \frac{1}{\sum_{i,j,i>j} |J_{ij}|} \sum_{i,j,i>j} r_{ij}|J_{ij}| \tag{14.7}$$

In the mean field picture, this must be the *true* average jump length.

14.2.2 II: Net current in direction of electric field

Exchanging the $N(\Delta x)$, with the $J(\Delta x)$, the total current with displacement Δx in the x-direction:

$$J(\Delta x) = \sum_{\left\{ \substack{i,j,where \\ \Delta x_{ij} = \Delta x} \right\}} |J_{ij}| \tag{14.8}$$

Then,

$$J_T(\Delta x) = J(-\Delta x) - J(\Delta x) \tag{14.9}$$

For each $J_T(\Delta x)$, there is an average jumplength:

$$\langle r(\Delta x) \rangle = \frac{1}{J(\Delta x) + J(-\Delta x)} \sum_{\left\{ \substack{i,j,where \\ |\Delta x_{ij}| = \Delta x} \right\}} |J_{ij}| r_{ij} \tag{14.10}$$

The average jump length is then:

$$\langle r \rangle_{II_{(MF)}} = \frac{1}{\sum_{\Delta x=1}^{10} J_T(\Delta x)} \sum_{\Delta x=1}^{10} J_T(\Delta x) \langle r(\Delta x) \rangle \tag{14.11}$$

14.3 Results and Discussion

We calculate $\langle r \rangle$ for both mean field and Monte Carlo data, using the both definitions, I and II, in sections 14.1 and 14.2.

For Monte Carlo results, we calculate $\langle r \rangle$ at temperatures T=0.03, 0.035, 0.04, 0.5, 0.6, 0.7, 0.8, 0.9, 0.1, using 18, 12, 7, 5, 3, 3, 3, 3, 3 different disorder configurations respectively. The Monte Carlo results were obtained by running simulations for $3 \cdot 10^6$ jumps from a random initial configuration, omitting the first million jumps.

The mean field results are obtained by averaging over 10 solutions for each temperature, each of a different disorder configuration.

As we see in figure 14.1, for mean field, both methods yield approximately a $(c/T)^p$-dependence on temperature. The fit to this function is somewhat better for method $II_{(MF)}$ which gives $p = 0.52$, while method I gives $p = 0.46$.

Method $II_{(MF)}$ gives consistently higher results for the average jump length than $I_{(MF)}$. Thus, the jump lengths of currents in the 'wrong' direction or with $\Delta x = 0$ tend be shorter than those in the 'right' direction. For mean field, the difference between $\langle r \rangle_{I_{(MF)}}$ and $\langle r \rangle_{II_{(MF)}}$ become smaller at increasing temperature, as $c = 0.21$ for method $II_{(MF)}$, and $c = 0.27$ for method $II_{(MF)}$.

The Monte Carlo results show that only method $II_{(MC)}$ gives an increase in jump length with lower temperatures at temperatures below $T \sim 0.6$. This increase is strong only at the lowest temperatures, from T=0.04 to T=0.03.

In contrast, method $I_{(MC)}$ gives a consistent *decrease* for all temperatures. This decrease is also seen, although somewhat weaker, in the results for method $II_{(MC)}$ from T=0.07 to T=0.1.

From the Monte Carlo set of results, which is small and with large uncertanties (see figure 14.2), it is difficult to infer any explicit law. It is however clear, for these results, that any $(c/T)^p$-dependence cannot be followed in the entire temperature range.

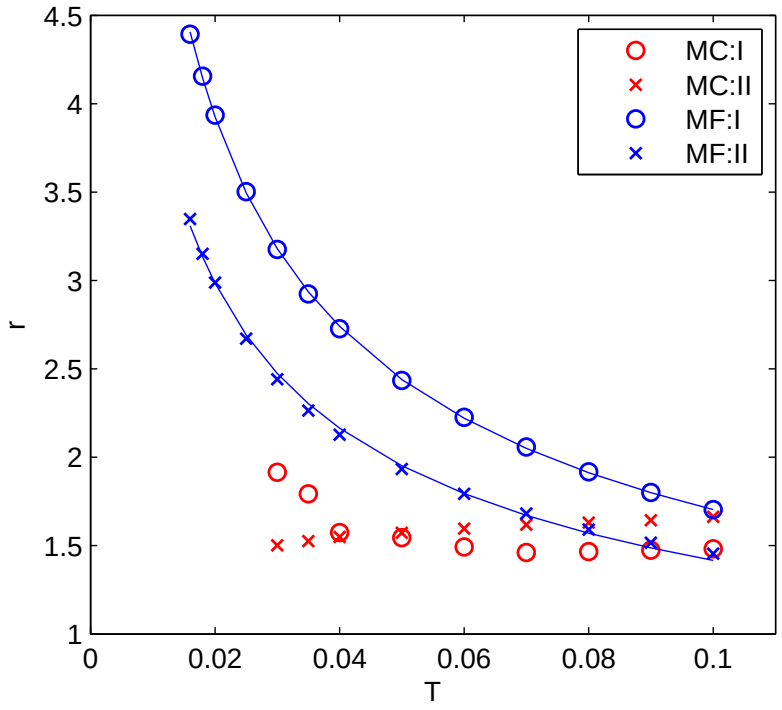

Figure 14.1: The average jump length using different definitions in sections 14.1.1-14.2.2 Markers are, for each temperature, averages of different disorder configurations, the number specified above.
Solid lines are fits to the function $f = -(c/T)^p$, where c, p are fitting parameters. These fits yield $p = 0.463 \pm 0.014$, $c = 0.21$ for MF, I and $p = 0.518 \pm 0.003$, $c = 0.27$ for MF, II.

By considering figures 14.2 and 14.3, it is obvious that at the lower temperatures, there is a large uncertainty in the results using method II_{MC}. $N_T(\Delta x)$ fluctuates wildly from sample to sample. At T=0.03, it is often negative. Still, there is a clear tendency that the longer jumps become more important at the lower temperatures.

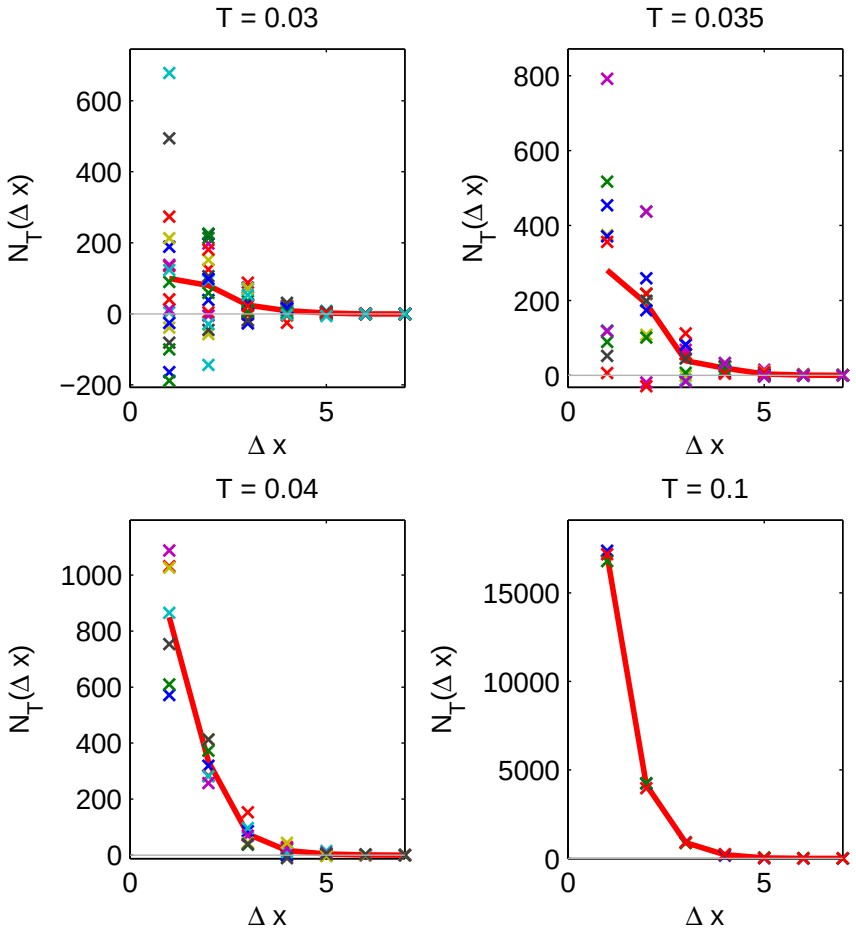

Figure 14.2: Monte Carlo simulations: Crosses: The net number of jumps $N(\Delta x)$ for different Δx. Color corresponds to different simulations.
Red Line: The average of $N(\Delta x)$ at Δx.

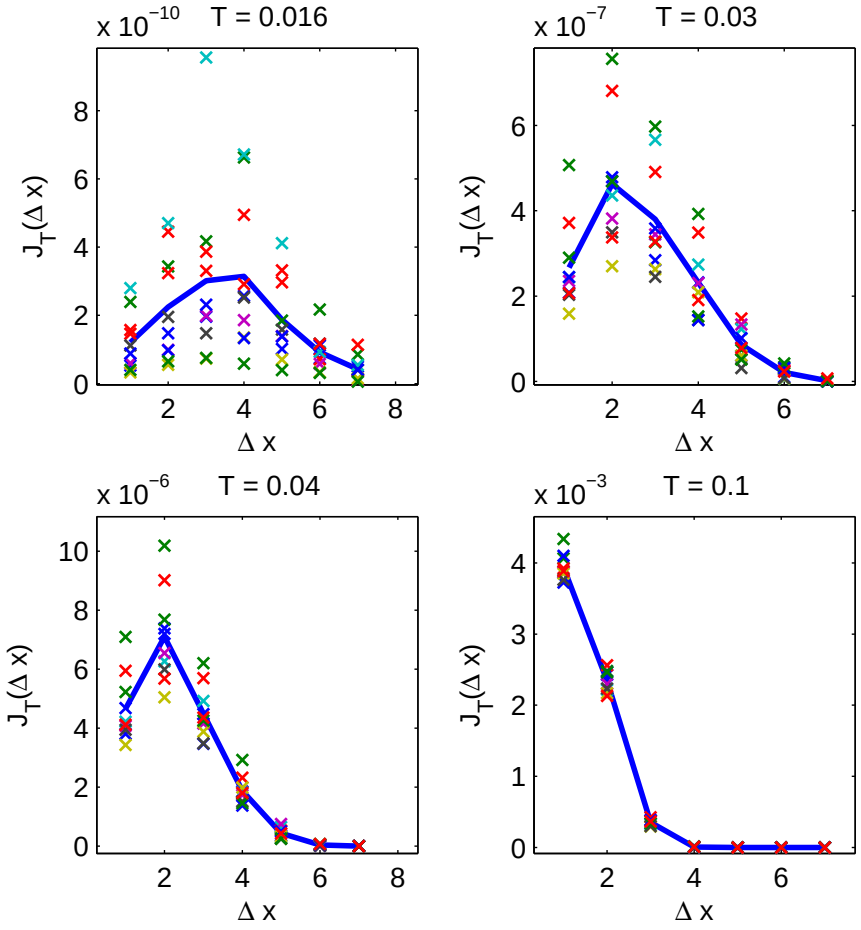

Figure 14.3: Mean field solutions: Crosses: The current $J_T(\Delta x)$ for different Δx. Color corresponds to different solutions of the resistance network.
Blue Line: The average of $J_T(\Delta x)$ at Δx.

15 Mapping of Currents

Having studied various properties of the MC and MF solutions, it is interesting to see how these play out in current mappings. In the following, we draw currents between sites as lines. The coloring of each line is chosen depending on the distance between sites, as specified in figure 15.1.

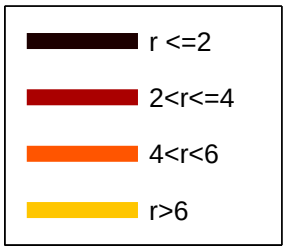

Figure 15.1: Coloring of lines in figure 15.3, 15.4, 15.6 determined by the distance between sites.

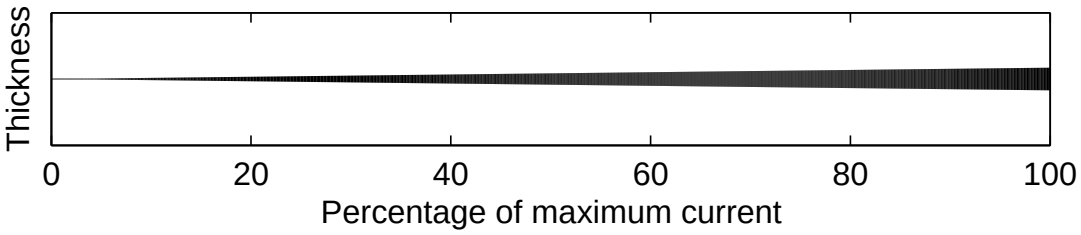

Figure 15.2: Thickness of lines in figure 15.3, 15.4, 15.6 determined by the fraction jumps/currents to the maximal current between sites.

The thickness, see figure 15.2, of each line between sites i and j is determined by the ratio of current to the maximum current between sites in the entire lattice.

15.1 Mean field currents

First, we want to investigate how different solutions at the same temperatures will appear in the mapping. Figure 15.3 shows four solutions solved from different inital values at T = 0.016. The plots are similar with regards to jump lengths and distribution of current flow, but in detail, they appear different.

Next, Figure 15.4 shows how temperature affect the currents. At high temperatures, current is distributed evenly over the lattice. Lowering the temperature, the tendency

is toward longer jumps and some main routes of current. At $T = 0.016$, we see in figure 15.3 that this tendency continues, with entire domains of the lattice practically without current.

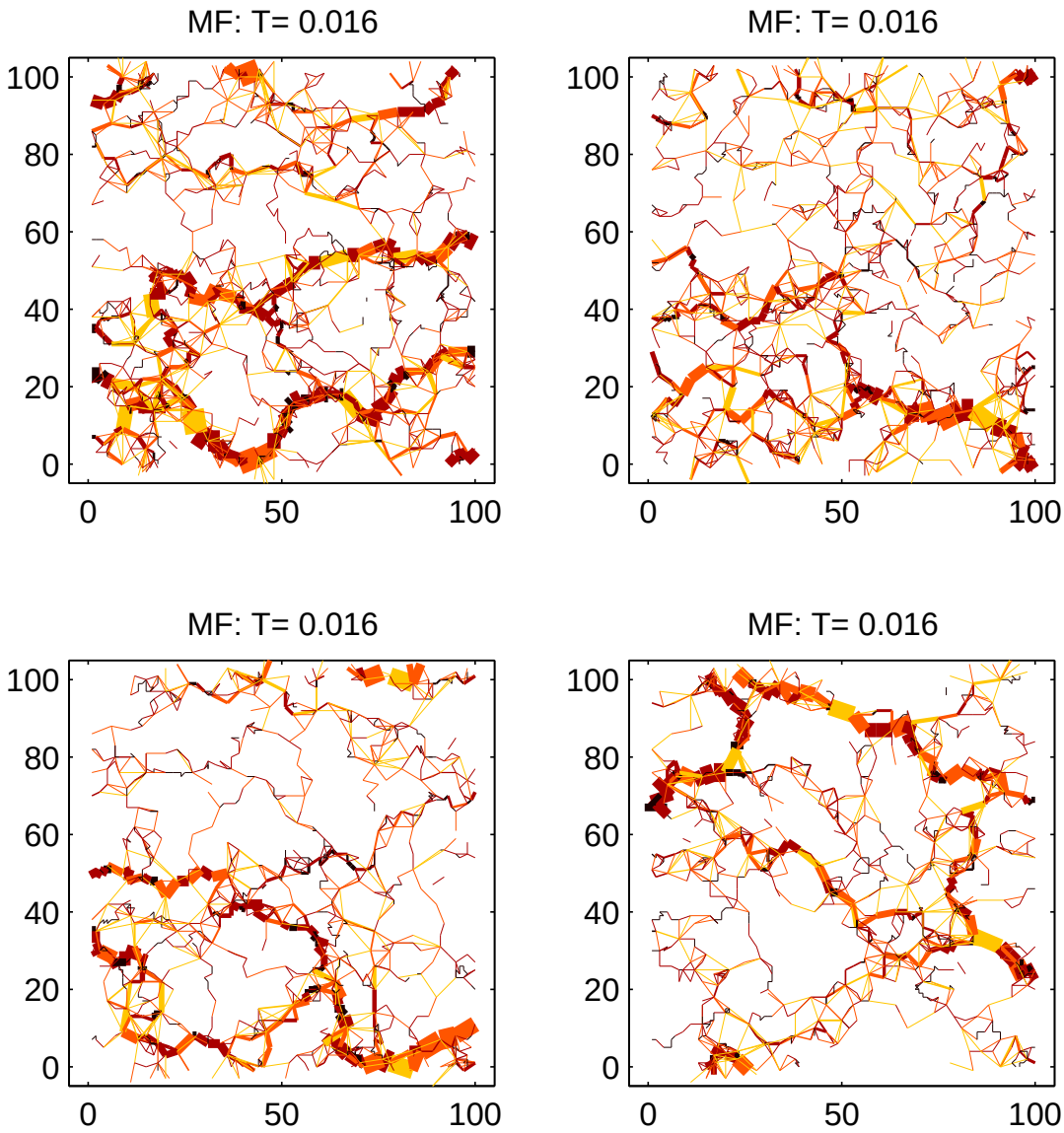

Figure 15.3: Currents calculated from four solutions of the mean field equations. Currents smaller than $1 \cdot 10^{-3}$ of the maximum current are omitted.

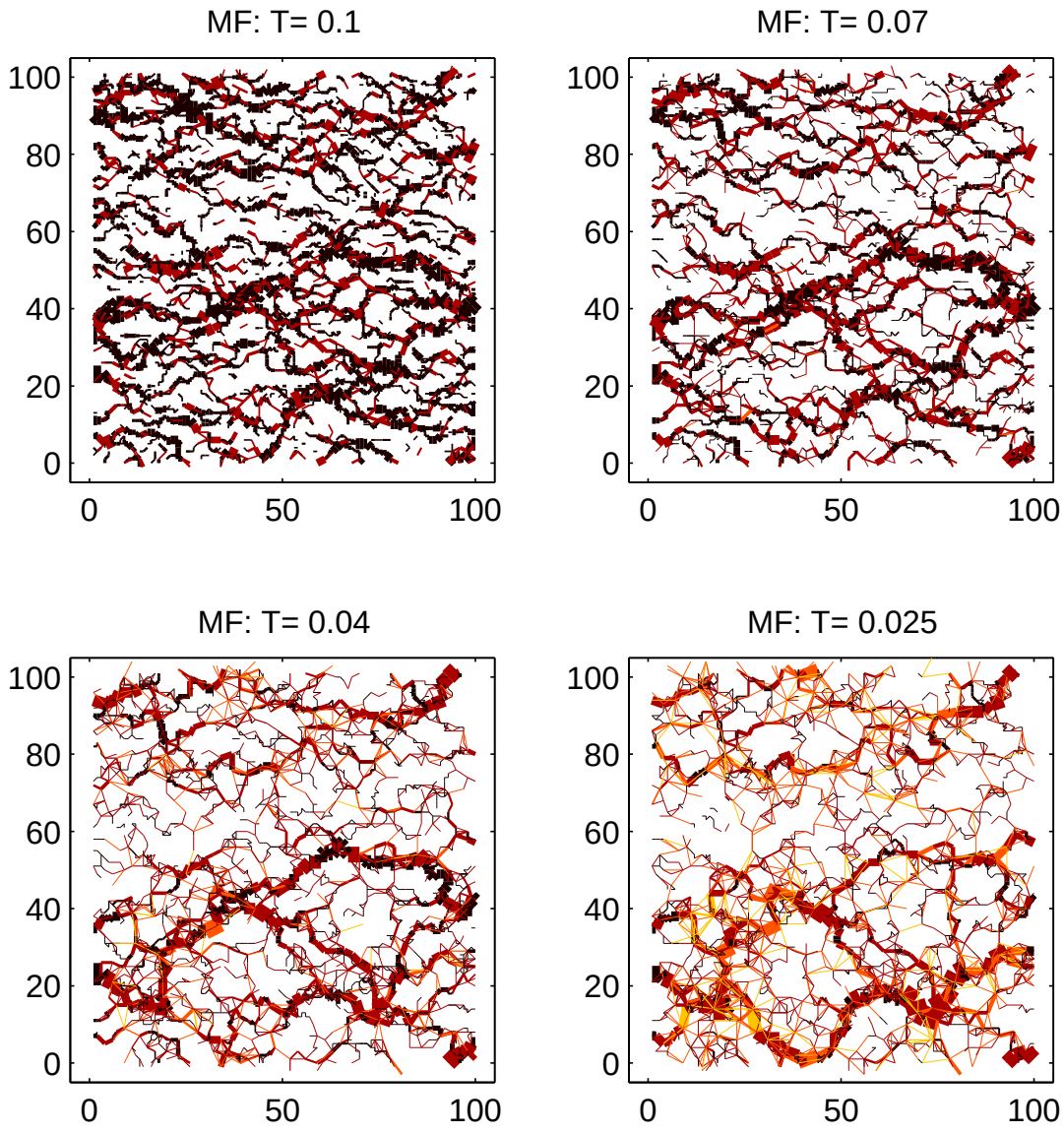

Figure 15.4: Currents at four temperatures, where the solutions to the mean field equations are found by lowering the temperature in steps, and using the solution at each temperature as the initial values at the lower temperature. Currents smaller than $1 \cdot 10^{-3}$ of the maximum current are omitted.

15.2 Monte Carlo currents

As discussed in section 14.1, extracting the jumps that contribute to current is challenging, as these jumps make up only a small fraction of the total number of jumps. For mapping of Monte Carlo currents, we use the following approach:

- 1: Identify the individual electron motion. In other words, find the complete path of each electron during the simulation.
- 2: For each path, smooth the motion by removing fluctuations. Specifically, this is done by eliminating all jumps where the net distance travelled is zero. For example: If the motion is between sites labelled i, j, k, l: The path $i \to j \to k \to i \to l$ is reduced to $i \to l$.
- 3: For each pair of sites, the current between is drawn and scaled with the accumulated, for all electrons, number of jumps, between the two.

Another approach to plotting currents is using *net jumps between sites*, as described in section 14.1.1. For comparison, figure 15.5 shows the net jumps and the jumps using the method of electron paths, compared to *all* jumps. The plots indicate that the current flow is more clear using the method of electron paths, while the method using net jumps between sites shows considerably more noise.

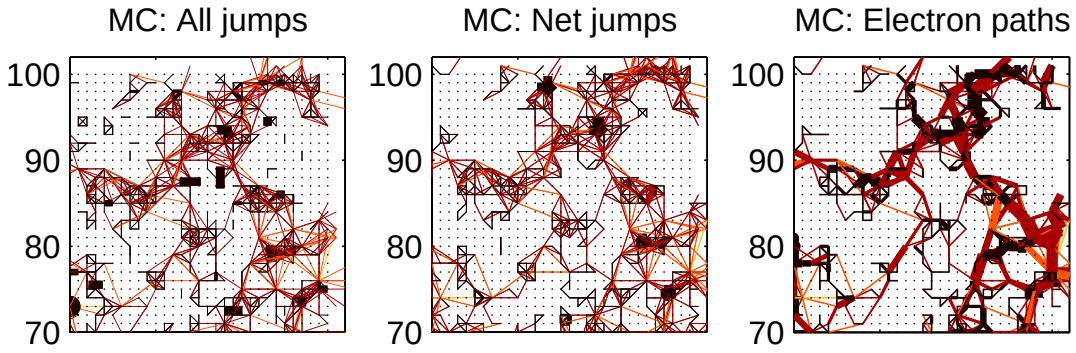

Figure 15.5: Zoom-in of jumps in lattice at $T = 0.025$. Left: All jumps. Middle: Net number of jumps between sites. Right: Smoothed Electron paths. The Monte Carlo data consists of a total of $15 \cdot 10^6$ jumps, of which 162264 and 14949 remains (in entire lattice) in the middle and right plot respectively. This compares to a net total displacement of electrons $\Delta x = 1432$.

15.3 Comparison between MC and MF currents

Despite the discrepancies between mean field and Monte Carlo solutions, discussed in previous sections, it is still interesting to see if the current paths in mean field theory and Monte Carlo simulations have similarities, or if they are completely different. It must be noted that some of these differences can be attributed to the models, since the Monte Carlo and mean field models are subject to different boundary conditions in the x-direction.

Since each solution of the mean field solution yields a different current flow, we try to find a solution that 'correspond' to a Monte Carlo solution.

We extract jumps from a point where the Monte Carlo simulation has equilibriated. The configuration at this point is used in solving the mean field equations. This is done for one temperature, $T = 0.025$.

In figure 15.6 it is difficult to see similarities with respect to current flow. The Monte Carlo currents is obviously obscured by a large amount of noise. Still, we see that the mapping shows a cluster extending from side to side. The jump lengths in this cluster are on average shorter than in the mean field mapping.

In comparison, the main mean field current paths are easy to identify, consisting of fewer, relatively long jumps. These long jumps ($r_{ij} > 6$) are rare in Monte Carlo simulations, and seemingly not necessary for the formation of a path across the sample.

There are some regions in the lattice where both maps show that current is absent, in some places more convincing than others.

Figure 15.7 and 15.8 show zoom-ups of a region where there seems to be a clear correspondence between Monte Carlo and mean field results, clearly showing how jumps in electrons in Monte Carlo simulations are shorter and more varied than mean field currents.

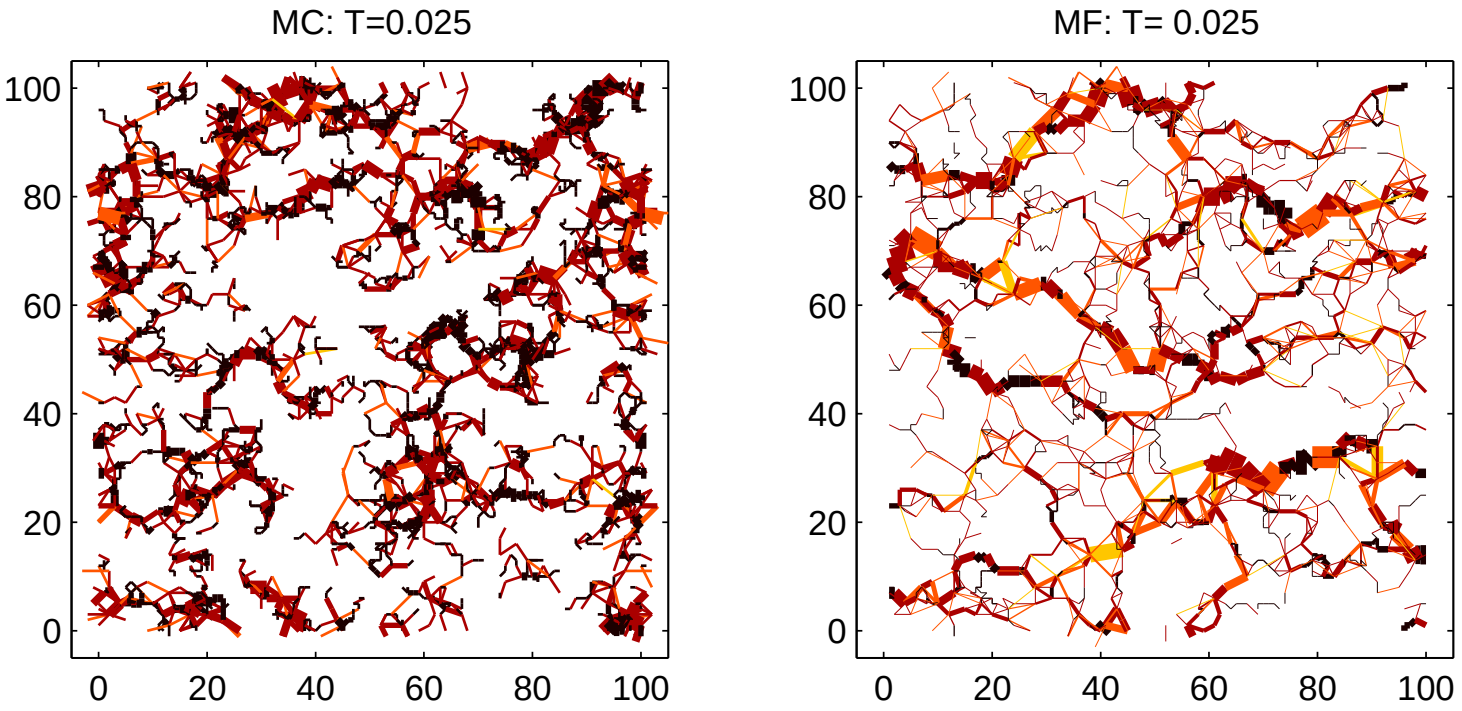

Figure 15.6: Monte Carlo and mean field currents at T=0.025. Left: Mean field currents.
Right: Monte Carlo results. The lines are electron paths found by the procedure in section 14.1, drawing only electrons with a net displacement in the direction opposite of the electric field. The currents are found from a total of $15 \cdot 10^6$ jumps.

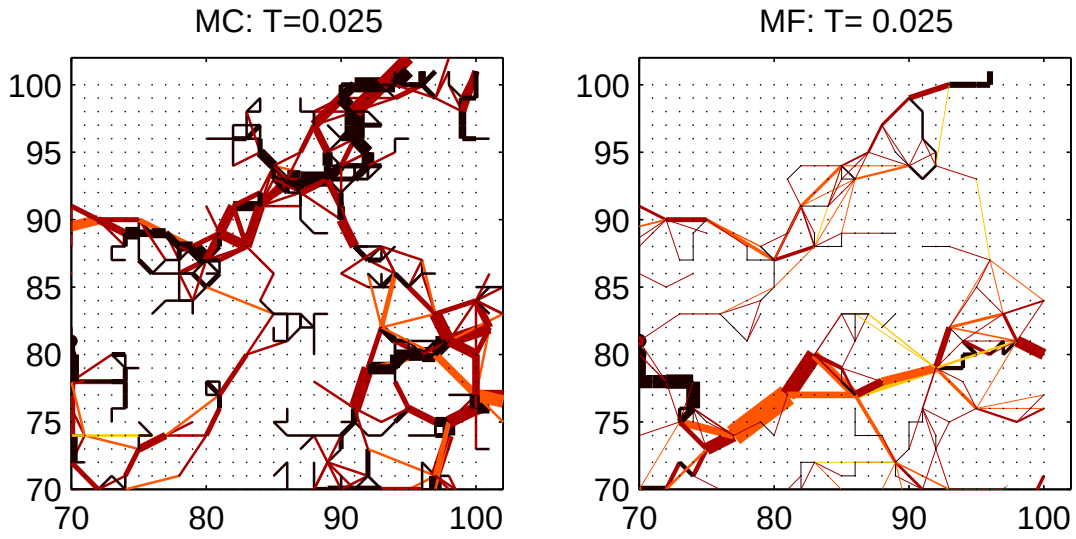

Figure 15.7: Zoom-in on the right top corners of plots in figure 15.6.

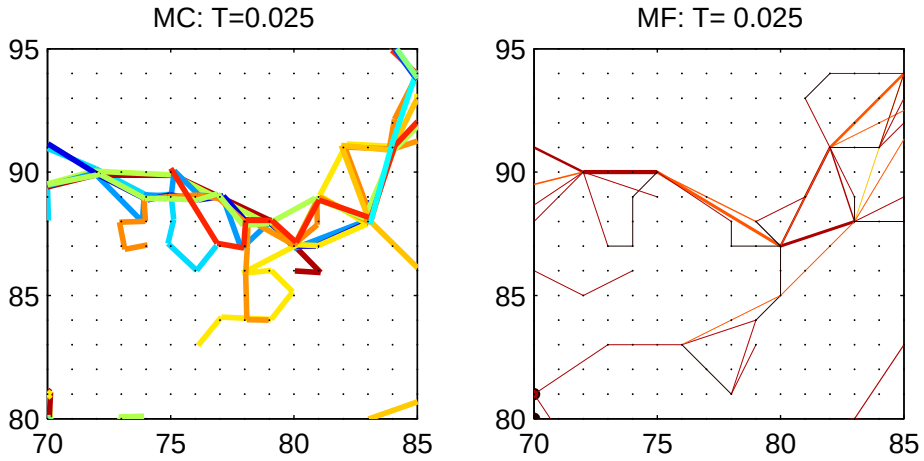

Figure 15.8: Closer zoom-in on figure 15.7. In left plot: Individual paths drawn with different colors. Only paths with a net displacement $\Delta x < -5$ are draw. The start and end points of lines have been slightly shifted, in order to differentiate between individual paths.

Part V
Discussion

The purpose of this work has been to compare mean field methods to Monte Carlo simulations in Coulomb glasses.

Two forms of the mean field transition rates were used, one a more sophisticated, modified, form of the other. In section 10 it was shown that only the modified version could give a satisfactory account of transitions from negative to positive energy states.

These transitions are not insignificant in the calculation of conductivity, as we showed in section 12: The resistor networks based on the modified transition rates yield a smaller value of β in $T_0 = \beta/a$ than the unmodified resistor network. Still, the conductivity of both networks were found to largely follow the Efros-Shklovskii law.

While the modified resistor network certainly is in better agreement with Monte Carlo simulations, it is far from perfect. After all, it is an approximation where all correlations, other than pair-correlations, in effect are ignored.

At the lowest temperatures, the consequences of the mean field approximation can perhaps most easily be understood. Here, averaged quantities such as the density of states and transition rates are in close agreement with Monte Carlo results: As figure 9.1 shows, at T=0.01, the density of states are nearly the same for mean field and Monte Carlo results. Figure 10.2 shows the total modified mean field transition rates are nearly the same as in Monte Carlo simulations, while figure 10.5 shows that relative to all transitions, the distribution of jump lenghts is also in agreement with Monte Carlo results.

Even though such equilibrium properties are in agreement, conductivity is still underestimated by several decades. We showed in section 14 that this underestimation can be related to a difference in hop lengths of currents: Jumps, on average, are longer in mean field results. This difference was corroborated by mappings of the current in section 15.3.

Another source of disagreement between the Monte Carlo and mean field conductivities, which we have not paid much attention to, is the different boundary conditions in the x-direction. It is possible that the electrons in the Monte Carlo simulations are somewhat freer, with more options, when they reach the boundary, while the mean field electrons are 'forced' into paths of higher resistance.

This effect possibly leads to an error in the value of β or σ_0 for the mean field results. It should however not influence the average jump length noticeably. A more sophisticated model would incorporate connections to leads at the boundaries.

References

[1] Ariel Amir, Yuval Oreg, Yoseph Imry, *Variable range hopping in the Coulomb glass.* Physical Review B, 80, 245214, (2009)

[2] Ariel Amir, Yuval Oreg, Yoseph Imry, *Mean-field model for electron-glass dynamics* Physical Review B, 77, 165208, (2008)

[3] Charles Kittel, *Introduction to Solid State Physics* ISBN: 978-0-471-41526-8, 0-471-41526-x, 0-471-68057-5

[4] B.I. Shklovskii, A.L. Efros *Electronic Properties of Doped Semiconductors.* ISBN: 0-387-12995-2, 3-540-12995-2 (1984)

[5] P.W. Anderson, *Absence of diffusion in certain random lattices.* Physical Review, 109, 1492 (1958)

[6] Allen Miller, Elihu Abrahams, *Impurity Conduction at Low Concentrations* Journal of Non-Crystalline Solids , 1, 1, (1968)

[7] R.F. Voss, *1/f noise and percolation in impurity bands in inversion layer.* Journal of Physics C, 11, L923 (1978)

[8] Don Monroue, A.C. Gossard, J.H. English, B. Golding, W.H Haemmerle, *Long-Lived Coulomb in a Compensated Semiconductor - The Electron Glass.* Physical Review Letters, 59, 1148 (1978)

[9] M. Kirkengen, J. Bergli, *Slow relaxation and equilibrium dynamics in a two-dimensional Coulomb glass: Demonstration of stretched exponential energy correlations.* Physical Review B 79, 075205, (2009)

[10] N.F. Mott *Conduction in Glasses Containing Transition Metal Ions* Physical Review, 120, 3, (1960)

[11] Aurora Voje, *Non-Ohmic Variable Range Hopping in Lightly Doped Semiconductors*, Master Thesis, University of Oslo (2009) (Available online at: `http://www.duo.uio.no/publ/fysikk/2009/94255/thesis.pdf`)

[12] D. N. Tsigankov, E. Pazy, B. D. Laikhtman, and A. L. Efros. *Long-time relaxation of interacting electrons in the regime of hopping conduction* Physical Review B, 68, 184205, (2003)

[13] S.D Baranovskii, A.L Efros, B.L Gel'mont, B.I Shklovskii, *Coulomb gap in disordered systems. Computer simulation.*

Solid State Commun. 27, 1, (1978)

[14] E.I. Levin, V.L. Nguen, B.I. Shklovskii, A.L. Efros, Sov. Phys. JETP, 68, 1081, (1989)

[15] F.G. Pikus and A.L Efros, *Critical Behaviour of Density of States in Diordered System with Localized Electrons.*

Physical Review Letters, 73, 22 (1994)

[16] J.Ruiz, M. Ortuno,E. Cuevas, V. Gasparian, Monte Carlo simulation of hopping conduction in two-dimensional Coulomb glasses

Journal of Physics: Condensed Matter, 7, (1995)